

---

## Bioconcentration, bioaccumulation and biomagnification of mercury in plankton of the Mediterranean Sea

Tesán-Onrubia Javier Angel <sup>1,\*</sup>, Heimbürger-Boavida Lars-Eric <sup>1,\*</sup>, Dufour Aurélie <sup>1</sup>, Harmelin-Vivien Mireille <sup>1</sup>, Garcia Arevalo Isabel <sup>2</sup>, Knoery Joël <sup>2</sup>, Thomas Bastien <sup>2</sup>, Carlotti François <sup>1</sup>, Tedetti Marc <sup>1</sup>, Bănaru Daniela <sup>1,\*</sup>

<sup>1</sup> Aix Marseille Univ, Université de Toulon, CNRS, IRD, MIO UM110, Marseille, France

<sup>2</sup> Ifremer, CCEM Contamination Chimique des Ecosystèmes Marins, F-44311 Nantes, France

\* Corresponding authors :

Javier Angel Tesán-Onrubia, email address : [javier.tesan@mio.osupytheas.fr](mailto:javier.tesan@mio.osupytheas.fr) ;

Lars-Eric Heimbürger-Boavida, email address : [lars-eric.heimburger@mio.osupytheas.fr](mailto:lars-eric.heimburger@mio.osupytheas.fr) ;

Daniela Bănaru, email address : [daniela.banaru@mio.osupytheas.fr](mailto:daniela.banaru@mio.osupytheas.fr)

---

### Abstract :

Plankton plays a prominent role in the bioaccumulation of mercury (Hg). The MERITE-HIPPOCAMPE campaign was carried out in spring 2019 along a north-south transect including coastal and offshore areas of the Mediterranean Sea. Sampling of sea water and plankton by pumping and nets was carried out in the chlorophyll maximum layer. Two size-fractions of phytoplankton (0.7–2.7 and 2.7–20 µm) and five of zooplankton (between 60 and >2000 µm) were separated, and their total mercury (THg) and monomethylmercury (MMHg) contents were measured. Bioconcentration of THg was significantly higher in the smallest phytoplankton size-fraction dominated by *Synechococcus* spp. The bioaccumulation and biomagnification of MMHg in zooplankton was influenced by size, food sources, biochemical composition and trophic level. MMHg was biomagnified in the plankton food web, while THg decreased toward higher trophic levels. Higher MMHg concentrations were measured in oligotrophic areas. Plankton communities in the Southern Mediterranean Sea had lower MMHg concentrations than those in the Northern Mediterranean Sea. These results highlighted the influence of environmental conditions and trophodynamics on the transfer of Hg in Mediterranean plankton food webs, with implications for higher trophic level consumers.

### Highlights

► Highest THg bioconcentration was highlighted in picoplankton. ► MMHg biomagnified while THg decreased along the plankton food web. ► MMHg bioaccumulated and biomagnified in zooplankton. ► Highest zooplankton MMHg concentrations were observed in oligotrophic areas.

**Keywords :** Mercury, Methylmercury, Plankton, Trophic transfer, Contamination, Food web

28

29 50

30

31 51 Mercury (Hg), predominantly in its inorganic form, is released to the atmosphere and the

32

33 52 ocean from natural and anthropogenic sources, with the latter largely outweighing the

34

35 53 former (Outridge et al., 2018). Anthropogenic Hg emissions are thought to have tripled

36

37 54 surface ocean Hg levels (Lamborg et al., 2014). Marine apex predator Hg levels are driven

38

39 55 by anthropogenic Hg inputs and marine methylmercury (MeHg) production (Medieu et al.

40

41 56 2022), yet their relative importance is still poorly constrained (Wang et al. 2019). The

42

43 57 relatively small and semi-enclosed Mediterranean Sea receives proportionally more Hg and

44

45 58 the sea water MeHg dynamics are well known, making it an ideal case study (Cossa et al.,

46

47 59 2022). Microorganisms present in the ocean can convert inorganic Hg into MeHg species

48

49 60 (Villar et al., 2020), namely monomethylmercury (MMHg) and dimethylmercury (DMHg).

50

51 61 MMHg is a potent neurotoxic which bioaccumulates in organisms with size and age and

52

53 62 biomagnifies in food webs, reaching high concentrations in apex predators (Morel et al.,

54

55 63 1998). Mediterranean human populations are exposed to high levels of Hg related to higher

56

57 64 marine fish consumption, posing a potential health risk (UNEP, 2019; Petrova et al., 2020).

58

59 65 This is further exacerbated by the higher fish Hg levels in the Mediterranean Sea, often

60

61 66 exceeding regulatory limits (Aston and Fowler, 1985; Storelli and Marcotrigiano, 2001;

62

63

64

65

66

67

68

69

67 Tseng et al., 2021).

68 Several hypotheses have been proposed to explain the so-called “Mediterranean Hg  
69 anomaly” (Aston and Fowler, 1985; Cossa and Coquery, 2005), mainly attributing the  
70 higher biota Hg levels to enhanced MeHg production. The high methylation capacities  
71 reported in the Mediterranean Sea may enhance MMHg availability to the lower trophic  
72 levels, namely plankton (Cossa and Coquery, 2005, Monperrus et al., 2007; Cossa et al.,  
73 2022). Similarly to the Arctic Ocean, the Mediterranean MeHg maxima are located at  
74 shallow depths in proximity to the phytoplankton habitat, allowing for an efficient uptake  
75 into the food web (Heimbürger et al., 2010, 2015; Cossa et al., 2012). Nevertheless, sea  
76 water Hg concentrations alone cannot explain the “Mediterranean Hg anomaly” observed for  
77 biota (Aston and Fowler, 1985; Cossa and Coquery, 2005). While Hg concentrations have  
78 been extensively observed in Mediterranean higher trophic level biota (Cinnirella et al.,  
79 2019 and references therein), only few studies have been conducted on plankton Hg levels  
80 (Cossa et al., 2012; Chouvelon et al., 2019).

81 Although studies are scarce, plankton organisms are hypothesized to play a key role in the  
82 accumulation and transfer of Hg in the Mediterranean food webs (Cossa and Coquery, 2005;  
83 Harmelin-Vivien et al., 2009; Chouvelon et al., 2018, 2019; Cossa et al., 2022).  
84 Phytoplankton bioconcentrates Hg more than 10,000 times from sea water, which is by far  
85 the largest enrichment step of Hg along the marine food web (Lee and Fisher, 2016).  
86 Mercury bioconcentration has been shown to be related to species and size, with the highest  
87 bioconcentration for smallest phytoplankton cells largely driven by their higher surface-to-  
88 volume ratio (Lee and Fisher, 2016). In the Mediterranean Sea, phytoplankton is mainly  
89 composed of small cells (pico- and nanoplankton) with a low biomass (Leblanc et al., 2018;  
90 Boudriga et al., 2022; Tesán-Onrubia et al., 2023), and a high Hg bioconcentration may thus  
91 be expected (Chouvelon et al., 2018). In addition, the slow-sinking pico- and  
92 nanophytoplankton cells are more prone to remineralization (Guidi et al., 2009) and thus to  
93 providing more Hg for methylation (Heimbürger et al., 2010). Due to technical difficulties,  
94 data on Hg concentrations in small phytoplankton fractions collected in the field remain  
95 scarce to date (Gosnell and Mason, 2015; Gosnell et al., 2017). Zooplankton represents the  
96 link between phytoplankton and higher trophic levels. MMHg bioaccumulates in  
97 zooplankton with size and age mainly because of food uptake (Tsui and Wang, 2004;  
98 Hammerschmidt et al., 2013). A size-based approach has become widely used to study the  
99 structure and functioning of the planktonic compartment (Rau et al., 1990; Rolff, 2000;

100 Carlotti et al., 2008; Hunt et al., 2017). However, taxonomic and groups composition differ  
101 between plankton size-fractions (Boudriga et al., 2023; Fierro-González et al., 2023).  
102 Zooplankton may exhibit different feeding patterns across size-fractions, ranging from  
103 herbivorous to carnivorous, resulting in different Hg exposure (Pućko et al., 2014).  
104 Oligotrophic ecosystems are characterized by lower growth rates, which reduces the  
105 biodilution of Hg in biota (i.e., decrease in Hg with increasing biomass) (Silva et al., 2008;  
106 Cossa et al., 2012; Chauvelon et al., 2018). The relatively warm waters of the Mediterranean  
107 Sea may stimulate Hg-methylating microbes (Bacci et al., 1989; Heimbürger et al. 2010),  
108 likewise increase the metabolic activity of higher trophic levels, and reduce excretion rates  
109 of MMHg (Remen et al., 2015; Maulvault et al., 2016). The biochemical composition of  
110 organisms can influence their physico-chemical affinity for Hg bioaccumulation (Wu and  
111 Wang, 2011; Charette et al., 2021). Overall, little is known about the biological mechanisms  
112 of accumulation of Hg in plankton in the Mediterranean Sea and the influence of species,  
113 size, and biochemical composition of plankton. Moreover, Hg biomagnification in the food  
114 web may be related to food sources but also to trophic structure. The longer food web of  
115 oligotrophic ecosystems (Décima, 2022; Tesán-Onrubia et al., 2023) may increase MMHg  
116 biomagnification (Cossa et al., 2012, 2022). Nevertheless, to date, biomagnification in a  
117 size-fractionated plankton food web has, to our knowledge, never been studied.  
118 The Mediterranean Sea represents a semi-enclosed basin with spatial nutrient gradients and  
119 different sources and concentrations of Hg in sea water (Durrieu de Madron et al., 2011;  
120 Cossa et al., 2022). Spatial variations of Hg concentrations have been shown in both sea  
121 water and sediments (Cossa and Martin, 1991; Horvat et al., 1999; Covelli et al., 2001;  
122 Tessier et al., 2011; Rosati et al., 2020), potentially impacting Hg concentrations in fishes  
123 (Kucuksezgin et al., 2001; Cresson et al., 2015) and at all levels of the food web (Chen et  
124 al., 2008). Gosnell and Mason (2015) hypothesized that the spatial variability of Hg  
125 concentrations in plankton size-fractions is also related to the plankton productivity.  
126 However, in the Mediterranean Sea, no spatially resolved data is available on the Hg content  
127 of plankton.  
128 To investigate the “Mediterranean Hg anomaly” at the base of the pelagic food web,  
129 sampling different plankton size classes remains a challenge, the main technical difficulty  
130 being the collection of large quantities for subsequent chemical analyses. A key feature of  
131 the MERITE-HIPPOCAMPE campaign was the implementation of targeted sampling  
132 strategies for the collection of large quantities of size-fractionated phyto- and zooplankton at

133 the chlorophyll maximum layer (CML). Throughout the MERITE-HIPPOCAMPE cruise,  
134 samples were taken for sea water, different size-fractions of phyto- (0.7–2.7, 2.7–20  $\mu\text{m}$ )  
135 and zooplankton (60–200, 200–500, 500–1000, 1000–2000 and >2000  $\mu\text{m}$ ). Complementary  
136 studies were also conducted on environmental parameters, species or groups composition,  
137 biochemical and stable isotopes composition of the different size-fractions (Boudriga et al.,  
138 2022; Fierro-González et al., 2023; Tesán-Onrubia et al., 2023; Tedetti et al., 2023). The aim  
139 of our study was to investigate the bioconcentration, bioaccumulation and biomagnification  
140 of THg and MMHg in different plankton size classes in contrasted ecoregions of the  
141 Mediterranean Sea.

## 143 2. Material and methods

### 145 2.1 Sampling preparation

147 The MERITE-HIPPOCAMPE cruise took place in the Mediterranean Sea, between April  
148 13th and May 14th 2019, onboard the R/V *Antea* (Fig. 1; Tedetti and Tronczynski, 2019). A  
149 total of 10 stations were sampled in different ecoregions, including coastal sites in the Bay  
150 of Marseille and Toulon (France), in the Gulf of Gabès (Tunisia) and offshore  
151 Mediterranean waters (Table S1). Details on the sampling sites, the hydro-bio-geochemical  
152 context and the sampling techniques are reported in Tedetti et al. (2023).

153 Unfiltered sea water was collected under trace metal clean conditions with a 12 L GOFLO  
154 bottle (General Oceanics). Sea water was filtered through a PFA filter holder (Savillex),  
155 holding a 47 mm diameter glass fiber filter of 0.7  $\mu\text{m}$  porosity (GF/F, Whatman), conserved  
156 in PFA bottles and immediately analyzed. Suspended particulate matter was sampled using  
157 McLane Large Volume Water Transfer System Samplers (WTS6-142LV, 4–8 L  $\text{min}^{-1}$ ), also  
158 called *in situ* pumps. These *in situ* pumps were mounted with bulk and sequential filtration  
159 systems (Bishop et al., 2012), holding 142 mm diameter nylon (20  $\mu\text{m}$ ), GF/D (2.7  $\mu\text{m}$ ) and  
160 GF/F (0.7  $\mu\text{m}$ ) filters, and typically filtered between 169 and 300 L. The glass fiber filters  
161 (GF/D and GF/F, Whatman) were pre-combusted (450°C, 6 h), rinsed, dried and weighed  
162 prior to deployment. The 20  $\mu\text{m}$  nylon filters (Mougel, France) were cleaned (HCl 0.05%  
163 v/v), dried and weighed prior to deployment. After deployment, the filters were stored  
164 folded in half in pre-combusted aluminum foil at –20°C.

165 Zooplankton collection was carried out towing a Multinet Plankton Sampler (Midi type with

166 0.25 m<sup>2</sup> opening, Hydro-Bios) at ~2 knots. The obtained bulk sample was consecutively  
167 sieved to obtain the following fractions: 60–200, 200–500, 500–1000, 1000–2000 and  
168 >2000 µm. Samples were stored in cleaned polypropylene tubes and conserved frozen at –  
169 20°C. In the laboratory, filters and zooplankton were freeze-dried before being analyzed.  
170 Overall, 67 samples were collected for THg and MMHg measurements in different fractions.  
171 We collected 10 samples of sea water, 10 samples of each of the following fractions: 0.7–  
172 2.7, 2.7–20, 60–200, 200–500 µm, 9 samples of the 500–1000 µm fraction, 5 samples of the  
173 1000–2000 µm fraction and 3 samples of the >2000 µm fraction.  
174 Dry weight biomass and biochemical content of all the sieved size-fractions were analyzed  
175 and are available in Tesán-Onrubia et al. (2023).

176

## 177 **2.2 Reagents and standards for Hg analyses**

178

179 Reagent and standard solutions were prepared in ultrapure water (18 MΩ cm; MilliQ).  
180 Sodium tetraethylborate (Merseburger Spezialchemikalien) solution (1% m/v) was prepared  
181 in ultrapure water and dispensed into 15 mL trace metal grade polypropylene vials (VWR).  
182 The solution was frozen initially and, after thawing, stored at 4°C for up to 3 days. Sodium  
183 acetate buffer solution (2 M) was prepared by diluting glacial acetic acid (J.T. Baker) and  
184 anhydrous sodium acetate (J.T. Baker), which was muffled at 300°C for 3 h prior to making  
185 up the solution. Nitric acid (14 M) and hydrochloric acid (12 M) were bi-distilled in a clean  
186 room under trace metal free conditions.

187 Standard solutions of inorganic Hg (iHg) (0.9 µg L<sup>-1</sup>) and MMHg (0.02 and 1 µg L<sup>-1</sup>) for  
188 plankton analysis were prepared from standard solutions (NIST3133 for iHg and a 1 µg L<sup>-1</sup>  
189 MMHg solution purchased from Brooks Rand Labs, traceable to NIST3133). The standards  
190 were diluted in 0.5% v/v nitric acid and 0.2% v/v hydrochloric acid solution using a  
191 precision balance (Mettler Toledo XS105; d = 0.01 mg).

192

## 193 **2.3 THg and MMHg in sea water**

194

195 Filtered dissolved total mercury (dHg) was analyzed on board by cold vapor atomic  
196 fluorescence spectrometry (CV-AFS) immediately after sampling. The mineralization of all  
197 dissolved Hg species was done using an acidic BrCl solution during 20 to 60 min prior to the  
198 analyses. For shipboard analyses, we used a lab-built sample sparging device connected to a

199 Tekran 2500 fluorescence detector and a chromatography package to quantify fluorescence  
200 peaks. For our analyses, a 40 mL aliquot of the digested sample containing its quantitatively  
201 oxidized mercury ( $\text{Hg}^{2+}$ ) was placed in a gas-stripping FEP tube. An excess of  $\text{SnCl}_2$  was  
202 added immediately before closing it to convert all Hg into gaseous elemental Hg,  $\text{Hg}(0)$ . The  
203 sample was sparged in a FEP tube at  $150 \text{ mL min}^{-1}$  for 4 min with Hg-free Ar to exsolve  
204  $\text{Hg}(0)$  and to sweep it toward a gold trap where it was retained. Mercury was thermally  
205 desorbed from the trap and swept by an argon stream into the CV-AFS detector. For dHg  
206 analyses, the daily 4-point external linear calibration curves were verified with an aliquot of  
207 a certified reference material (ORMS-5, National Research Council Canada) that was  
208 analyzed every fifth run. Additional 1-point recalibration curves were acquired when the  
209 instrument's response drifts by more than 5% from the target value of the reference material.  
210 Overall precision and accuracy of dHg measurements, based on repeated analyses of  
211 samples, standards and CRMs, was better than 10%, and limits of quantification attained  
212 during the cruise were better than  $5 \text{ pg L}^{-1}$ , based on repeated analyses of  $4 \text{ pg Hg}^{2+}$ .  
213 Unfiltered MeHg species were analyzed back at the laboratory in samples acidified to 0.5%  
214 v/v with HCl 11N, and stored in FEP bottles without headspace. Acidification converts the  
215 gaseous DMHg to MMHg, and thus the sum of both is measured as MeHg. The general  
216 principles of the hydride generation are as follows. Analyses were carried out by sparging a  
217 40 mL sample aliquot with He while  $\text{NaBH}_4$  was continuously added ( $10 \text{ g L}^{-1}$  pumped at  
218  $0.25 \text{ mL min}^{-1}$ ). The evolved volatiles were retained on a 20 cm long, U-shaped cryogenic  
219 trap and chromatography column (Chromosorb with silicone OV1 at 15%) immersed in  
220 liquid nitrogen. When stripping of the MeHg is completed after 7 min, the trap is removed  
221 from liquid nitrogen and heated. As it progressively warms, the trapped Hg species  
222 including elemental and MeHg are released at different times from the column. Helium and  
223 Hg gases exiting from the outlet of the column then flowed through a 20 cm x 1 mm inner  
224 diameter quartz tube maintained at  $800^\circ\text{C}$ , where Hg species are pyrolyzed to elemental Hg.  
225 The cooled helium and Hg vapor were then directed to a mirrored cell (Hellma, Germany) of  
226 a CV-AFS detector (Tekran 2500).

227 A 2-point external calibration was done at the beginning of each day, and after every 5th  
228 sample to account for potential instrumental drift. Based on the uncertainty of low amounts  
229 of analyte ( $2 \text{ pg Hg}$  as MMHg), the detection limit was  $0.29 \text{ pg Hg}$  as MMHg, in a 40 mL  
230 sample ( $7 \text{ pg L}^{-1}$ ). The dissolved methylmercury (dMeHg) species were calculated by  
231 subtracting the particulate ( $0.7$  to  $20 \text{ }\mu\text{m}$ ) from the unfiltered fraction.

232

## 233 2.4 THg and MMHg in plankton

234

235 THg was analyzed in zooplankton size-fractions ( $>60\ \mu\text{m}$ ) using atomic absorption  
236 spectrometry (AAS, AMA 254, LECO). The analyzer was equipped with a low-level Hg  
237 optical cell. The certified reference material (MESS-4, National Research Council Canada)  
238 was measured at the beginning and end of the run to verify accuracy. The THg  
239 measurements were always within the certified values and the limit of detection,  
240 corresponding to the blank plus three times the standard deviation, was 23 pg.

241 In contrast to zooplankton, THg and MMHg on digested filters were simultaneously  
242 measured by purge-and-trap gas chromatography pyrolysis atomic fluorescence  
243 spectrometry (PT-GC-Pyr-AFS, MERX-M, Brooks Rand Labs) (Sharif et al., 2013). The  
244 biomass collected on filters was too low for measuring THg in a subsample with a signal  
245 close to the detection limits of the AAS. Secondly, particulate matter may not be evenly  
246 distributed in the filters and may not be suitable for subsampling (Bishop et al., 2012).

247 Filters were digested, and both iHg and MMHg were derivatized and measured  
248 simultaneously. Briefly, filters and zooplankton aliquots between 13 and 190 mg were  
249 digested in 20 and 60 mL, pre-combusted ( $350^\circ\text{C}$ , 5 h) glass vials with 4.57 M nitric acid  
250 (3.5–15 mL) for 12 h at  $60^\circ\text{C}$  (Hammerschmidt and Fitzgerald, 2006). Amber glass vials (60  
251 mL) were filled with ultrapure water and buffered with sodium acetate to pH 4.5–4.9. An  
252 aliquot of the acidic extract (400–800  $\mu\text{L}$ ) was then added. The solution was spiked with iHg  
253 (100 to 400  $\mu\text{L}$ ) and MMHg (10 to 400  $\mu\text{L}$ ) solutions for quantification *via* standard  
254 addition.

255 Finally, we added the derivatizing agent, sodium tetraethylborate ( $\text{NaBeT}_4$ ) and filled the  
256 vial with ultrapure water until a slightly negative meniscus was formed. The cap was  
257 tightened, and the preparation was gently mixed. The samples were measured by PT-GC-  
258 Pyr-AFS. The chromatogram typically contains three peaks, corresponding to different  
259 mercury species: elemental mercury ( $\text{Hg}^0$ ), ethylmethylHg and diethylHg. THg was  
260 calculated as the sum of iHg and MMHg. We followed a standard addition protocol to  
261 estimate THg and MMHg concentrations. The low concentrations and matrix effect  
262 associated with biological samples make standard addition a more reliable analytical  
263 approach than external calibration. For a single sample, five measurements were performed  
264 to construct a regression line. Of the five measurements, two corresponded to sample



265 replicates without addition, and the remaining three to three different volumes of standard  
266 solution. The targeted standard volumes corresponded to between 1 and 5 times the amount  
267 of iHg or MMHg present in the sample. The linear regression between added iHg or MMHg  
268 and the peak height was calculated. The y-intercept of the linear regression was used to  
269 obtain the iHg and MMHg concentrations. The correlation coefficients ( $R^2$ ) ranged from  
270 0.96 to 1.00. The certified reference material (DORM-4, National research council Canada)  
271 was digested and measured similarly to the samples. The measurements corresponded  
272 respectively to 79 and 85% of the THg and MMHg certified concentrations. The limits of  
273 detection for iHg and MMHg were respectively 8 and 0.8 pg.

274 Based on the measurement made during the MERITE-HIPPOCAMPE cruise between  
275 plankton biomass wet and dry weights (% of water in plankton:  $90 \pm 3\%$ ; Tedetti et al.,  
276 2023), a factor of 10 was used to allow comparison of the THg and MMHg concentrations  
277 expressed here on a dry weight basis, with those reported in the literature. Further  
278 experiments were carried out to assess the THg blanks in the filters, which could be due to  
279 the retention of dissolved, colloidal and particulate Hg ( $<0.7 \mu\text{m}$ ) (Table S2). Different  
280 volumes of sea water (10–80 L) were filtered as replicates through three stacked  $0.7 \mu\text{m}$   
281 glass fiber filters (GF/F, 142 mm). THg blanks measured on the 2nd and 3rd filters were not  
282 significantly different ( $H = 1$ ;  $p > 0.05$ ) and represented less than 2% of the particulate  
283 fraction measured on the 1st filter ( $n = 12$ ). We therefore assume that the THg measured on  
284 the filters was representative of the particulate fraction, with a negligible contribution of the  
285 dissolved ( $<0.7 \mu\text{m}$ ) fraction.

286

## 287 2.5 Data treatment

288

289 The effect of size-fractions and geographical area on the THg, MMHg and fraction of  
290 MMHg were assessed by means of one-way ANOVA (F) or non-parametric Kruskal-Wallis  
291 (H) tests after testing for normality and homogeneity of variances, followed by appropriate  
292 paired comparison tests, using the software Statistica 12. Principal component analysis  
293 (PCA) was performed using the R software (R Core Team, 2017). The PCA used data from  
294 Tesán-Onrubia et al. (2023) that may influence THg and MMHg in zooplankton: proteins,  
295 carbohydrates, lipids,  $\delta^{13}\text{C}$ ,  $\delta^{15}\text{N}$ , C/N, THg and MMHg in the 0.7–2.7 and 2.7–20  $\mu\text{m}$   
296 fractions, phytoplankton size-fractions biomass, zooplankton size-fractions biomass, and  
297 plankton group composition.

298 The bioconcentration factor of THg and MMHg ( $BCF_{Hg}$ , in  $L\ kg^{-1}$ ) was calculated between  
299 plankton and sea water:

$$BCF_{Hg} = \left( \frac{[Hg]_{Plankton}}{[Hg]_{Seawater}} \right) \times 10^6$$

300 where  $[Hg]_{Plankton}$  is the dry weight concentrations of THg or MMHg on a given size-fraction  
301 (in  $ng\ g^{-1}$ ),  $[Hg]_{sea\ water}$  is the dissolved concentrations of Hg (dHg) or MeHg (dMeHg) in sea  
302 water (in  $pg\ L^{-1}$ ), and  $10^6$  is the unit conversion factor.

303 The trophic magnification factor ( $TMF_{Hg}$ ) of THg and MMHg was calculated within the  
304 planktonic food web as follows:

$$TMF_{Hg} = 10^a$$

$$\text{Log } [Hg]_{Plankton} = \delta^{15}N * a + b$$

307 where  $\log [Hg]_{Plankton}$  is the logarithm of the THg or MMHg concentration in plankton  
308 fractions,  $\delta^{15}N$  is the nitrogen stable isotope in the plankton fraction and  $a$  is the slope of the  
309 linear regression.

### 3. Results and discussion

314 The basis of marine Mediterranean food webs is mainly constituted of pico- (0.7–2.7  $\mu m$ ) and  
315 nanophytoplankton (2.7–20  $\mu m$ ) (Bănaru et al., 2013; 2019). These phytoplankton fractions  
316 are consumed by zooplankton (Hunt et al., 2017; Tesán-Onrubia et al., 2023), which transfer  
317 the organic matter and the associated contaminants up to higher trophic level consumers. THg  
318 and MMHg measurements on the 0.7–2.7 and 2.7–20  $\mu m$  size-fractions are scarce and were  
319 usually only measured on relatively small sea water volumes (Gosnell and Mason, 2015;  
320 Gosnell et al., 2017). In the present study, these analyses were performed on large volume  
321 samples (>150 L), which enabled precise Hg species measurements and complementary  
322 biological and biochemical analyses (Tesán-Onrubia et al., 2023).

#### 3.1 THg and MMHg in phytoplankton

325 A contrasted pattern of the relationship between concentration and size was observed for THg  
326 and MMHg in phyto- and zooplankton size classes (Fig. 2a, 2b, Tables S3, S4). Both THg and

327 MMHg concentrations decreased in phytoplankton with increasing cell size, but the difference  
328 was statistically significant only for THg in the smallest size-fractions ( $86 \pm 32 \text{ ng g}^{-1} \text{ dw}$  in  
329 the  $0.7\text{--}2.7 \mu\text{m}$  fraction, and  $42 \pm 28 \text{ ng g}^{-1} \text{ dw}$  in the  $2.7\text{--}20 \mu\text{m}$  fraction) ( $F = 10.6$ ,  $p =$   
330  $0.005$ ). These values were in the upper range (maxima  $42\text{--}160 \text{ ng g}^{-1} \text{ dw}$ ) of previous  
331 observations obtained on a wide range of phytoplankton fractions (Baeyens et al., 2003;  
332 Hammerschmidt and Fitzgerald, 2006; Beldożska and Kobos, 2018; Cossa et al., 2012;  
333 Hammerschmidt et al., 2013; Gosnell and Mason, 2015; Lamborg et al., 2016; Fox et al.,  
334 2017; Harding et al., 2018). However, our measurements were lower than the maxima ( $420\text{--}$   
335  $740 \text{ ng g}^{-1} \text{ dw}$ ) reported in studies with larger size-fractions (Bargagli et al., 1998), indirect  
336 measurements (Luengen and Flegal, 2009), small volumes of filtered sea water (Gosnell et al.,  
337 2017) and estuaries (Kehrig et al., 2009; Mason et al., 2021, 2023) (Table S5). Mean MMHg  
338 concentrations of  $1.2 \pm 0.7 \text{ ng g}^{-1} \text{ dw}$  and  $0.8 \pm 0.6 \text{ ng g}^{-1} \text{ dw}$  were measured in the  $0.7\text{--}2.7$   
339 and in the  $2.7\text{--}20 \mu\text{m}$  fractions, respectively, and are within the range of previous studies. Our  
340 observations correspond well to MMHg concentration measured in phytoplankton (Baeyens et  
341 al., 2003; Hammerschmidt and Fitzgerald, 2006; Luengen and Flegal 2009; Cossa et al., 2012;  
342 Hammerschmidt et al., 2013; Gosnell and Mason, 2015; Gosnell et al., 2017; Fox et al., 2017;  
343 Harding et al., 2018) but were lower than concentrations modeled for the Mediterranean Sea  
344 ( $2\text{--}15 \text{ ng g}^{-1} \text{ dw}$ ) (Rosati et al., 2022) and for the global ocean ( $12\text{--}185 \text{ ng g}^{-1} \text{ dw}$ ) (Zhang et  
345 al., 2020; Wu et al., 2021).

346 Chouvelon et al. (2019) showed that Hg bioaccumulation in the lowest size-fractions ( $6\text{--}60$   
347  $\mu\text{m}$ ) may be high compared to larger plankton size-fractions. The higher surface-to-volume  
348 ratio (giving a higher contact surface), which increases Hg uptake (Fisher, 1985), may explain  
349 the higher concentrations of THg measured in picoplankton in our study. Small phytoplankton  
350 cells are prevalent in Mediterranean oligotrophic waters and during our sampling survey  
351 (Boudriga et al., 2022). Enhanced concentrations of MeHg have previously been observed in  
352 sea water during pico- and nanoplankton blooms in the Mediterranean Sea (Heimbürger et al.,  
353 2010).

354 Low dissolved Hg (dHg) and MMHg (dMMHg) concentrations measured in this study ( $94 \pm 32$   
355  $\text{pg L}^{-1}$  and  $13 \pm 7 \text{ pg L}^{-1}$ , respectively, Table S6) are likely due to enhanced photochemistry  
356 and evasion (Cossa et al., 2009; Sunderland et al., 2009; Heimbürger et al., 2010; Cossa et al.,  
357 2022). The mean  $\text{BCF}_{\text{THg}}$  values in the  $0.7\text{--}2.7$  and  $2.7\text{--}20 \mu\text{m}$  fractions were  $2 \times 10^6 \text{ L kg}^{-1}$   
358  $\text{dw}$  and  $1 \times 10^6 \text{ L kg}^{-1} \text{ dw}$ , respectively, while the mean  $\text{BCF}_{\text{MMHg}}$  values were  $1 \times 10^5 \text{ L kg}^{-1}$   
359  $\text{dw}$  and  $8 \times 10^5 \text{ L kg}^{-1} \text{ dw}$ , respectively (Table S7). Mediterranean phytoplankton of different



360 size classes bioconcentrate THg and MMHg  $10^6$  and  $10^5$  times, respectively, from sea water,  
361 these values being in the upper range of those reported in the literature (Table S5). The mean  
362 THg bioconcentration values observed in this study are >10 times higher than the partitioning  
363 coefficient of suspended particulate matter ( $K_d$ ), generally used in global THg models (Zhang  
364 et al., 2014), which testifies to the need for more accurate regional data. Various studies have  
365 already highlighted the underestimation of  $K_d$ , constraining Hg export fluxes from the surface  
366 and, more broadly, its biogeochemical cycle (Lamborg et al., 2016; Tesán-Onrubia et al.,  
367 2020). It has also been observed that MMHg bioconcentration was promoted under low  
368 dissolved organic carbon concentrations (Schartup et al., 2018).

369 The MERITE-HIPPOCAMPE cruise offered a unique opportunity to couple biological and  
370 contaminant analyses (Tedetti et al., 2023), and explore for the first time the relationships  
371 between the composition of the suspended particles collected, and their THg and MMHg  
372 concentrations. Suspended particles collected on filters were a complex mixture of living and  
373 dead organisms (autotrophic and heterotrophic), also containing detritus and mineral particles.  
374 Tesán-Onrubia et al. (2023) showed that the 0.7–2.7 and 2.7–20  $\mu\text{m}$  size-fractions were  
375 dominated (86% of the total biomass) by two phytoplankton groups: *Synechococcus* spp. (~1  
376  $\mu\text{m}$ ) and nanoeukaryotes (~4  $\mu\text{m}$ ). The two axes of the PCA analysis relating THg and  
377 MMHg concentrations to the size class and group composition of phytoplankton explained  
378 56% of the variability (Fig. S1). Higher THg concentrations were associated with a  
379 dominance of *Prochlorococcus* spp. (~0.5  $\mu\text{m}$ ) in the 0.7–2.7  $\mu\text{m}$  size-fraction, and a  
380 dominance of nanoeukaryotes in the 2.7–20  $\mu\text{m}$  size-fraction. Similarly, higher MMHg  
381 concentrations were related to the dominance of *Synechococcus* spp. in the 0.7–2.7  $\mu\text{m}$  size-  
382 fraction, and to the dominance of *Cryptophyceae* (~6  $\mu\text{m}$ ) in the 2.7–20  $\mu\text{m}$  size-fraction.  
383 These two phytoplankton size-fractions constitute a large part of the diet of zooplankton  
384 organisms between 200 and 1000  $\mu\text{m}$  size, and represent an important source of Hg for  
385 consumers (Tesán-Onrubia et al., 2023).

### 3.2 THg and MMHg in zooplankton

389 THg and MMHg bioaccumulated with size among zooplankton, their concentrations  
390 increasing from 22 to 45  $\text{ng g}^{-1}$  dw, and from 3 to 7  $\text{ng g}^{-1}$  dw, respectively, in 60 to 2000  $\mu\text{m}$   
391 size-fractions (Fig. 2a, 2b, Tables S3, S4). Bioaccumulation of MMHg with zooplankton size  
392 was previously shown in the North Atlantic (Hammerschmidt et al., 2013), while no

393 difference was found for THg in the Mediterranean (Chouvelon et al., 2019). THg and MMHg  
394 concentration values reported here in the Mediterranean zooplankton were comparable to  
395 those observed in other regions (Table S8) (Stern and Macdonald, 2005; Hammerschmidt and  
396 Fitzgerald, 2006; Loseto et al., 2008; Lavoie et al., 2010; Cossa et al., 2012; Hammerschmidt  
397 et al., 2013; Gosnell and Mason, 2015; Gosnell et al., 2017; Harding et al., 2018), but were  
398 lower than those from the Arctic Ocean (Campbell et al., 2005; Foster et al., 2012; Pućko et  
399 al., 2014; Fox et al., 2017) and from one study in the Mediterranean Sea (Buckman et al.,  
400 2018). Our measured MMHg concentrations in zooplankton are in relatively good agreement  
401 with model outputs for the Mediterranean Sea (3–10 ng g<sup>-1</sup> dw) (Rosati et al., 2022) and the  
402 global ocean (1–69 ng g<sup>-1</sup> dw) (Zhang et al., 2020; Wu et al., 2021).

403 Changes in metabolism during an organism's life cycle may impact its MMHg concentration.  
404 Hammerschmidt and Fitzgerald (2006) showed reduced removal and higher uptake rates in  
405 large-size organisms compared to smaller ones. Fierro-González et al. (2023) reported an  
406 increase in carnivory with increasing size of zooplankton, which was also in agreement with  
407 increasing trophic level traced by  $\delta^{15}\text{N}$  (Tesán-Onrubia et al., 2023). The lowest THg and the  
408 highest MMHg concentrations were both measured in the largest size-fraction (>2000  $\mu\text{m}$ )  
409 (Table S3, S4 and S9), as observed in previous studies (Chouvelon et al., 2019).

410 The biochemical composition of zooplankton may also explain the accumulation of THg and  
411 particularly MMHg. MMHg concentrations were significantly correlated with particulate  
412 organic carbon (POC), proteins and lipids in zooplankton ( $R^2 = 0.47$ ,  $p < 0.0001$ ;  $R^2 = 0.18$ ,  $p$   
413  $= 0.009$  and  $R^2 = 0.25$ ,  $p = 0.002$ , respectively). The quantity of these compounds increased  
414 with the size of zooplankton, except for the >2000  $\mu\text{m}$  fraction (Tesán-Onrubia et al., 2023).  
415 The affinity of Hg for POC and proteins is due to the capacity of thiol groups present in  
416 cellular proteins to effectively bind to Hg and MMHg (Ravichandran, 2004; Yoon et al.,  
417 2005; Gosnell and Mason, 2015).

### 419 3.3 Trophic transfer of THg and MMHg

420 Trophic transfer in the plankton food web was assessed taking into consideration all phyto-  
421 and zooplankton size-fractions. The two smallest size-fractions of phytoplankton (0.7–2.7 and  
422 2.7–20  $\mu\text{m}$ ) presented the highest THg but the lowest MMHg concentrations with respect to  
423 most zooplankton size-fractions ( $H = 23.9$ ,  $p < 0.0001$  and  $H = 30.1$ ,  $p < 0.0001$ , respectively)  
424 (Fig. 2a, 2b, Tables S3, S4). While THg concentrations were related mainly to the effect of  
425 the surface-volume ratio on bioconcentration in phytoplankton, MMHg concentrations were



426 mainly related to predation relationships and biomagnification processes among zooplankton  
427 fractions. Biomagnification was assessed by using the  $\delta^{15}\text{N}$  as a proxy of trophic level (Fig.  
428 3). The logTHg and logMMHg showed respectively negative and positive correlations with  
429  $\delta^{15}\text{N}$  ( $R^2 = 0.1$ ,  $p < 0.05$  and  $R^2 = 0.43$ ,  $p < 0.0001$ , respectively,  $n = 57$ ), indicating a  
430 bioreduction of THg ( $\text{TMF}_{\text{THg}} = 0.9$ ) and a biomagnification of MMHg in the food web  
431 studied ( $\text{TMF}_{\text{MMHg}} = 1.7$ ). In our work, particularly low  $\text{TMF}_{\text{THg}}$  were recorded, indicating a  
432 marked bioreduction of THg within the planktonic food web. Chouvelon et al. (2009) also  
433 observed no THg increase in zooplankton fractions of increasing size, and THg  
434 biomagnification in the food web only when zooplanktivorous fishes were considered. In our  
435 case, when only zooplankton size-fractions  $>60 \mu\text{m}$  were considered, significant positive  
436 correlations were observed for both logTHg and logMMHg and  $\delta^{15}\text{N}$  ( $R^2 = 0.22$ ,  $p < 0.005$   
437 and  $R^2 = 0.39$ ,  $p < 0.0001$ , respectively), thus evidencing the biomagnification of THg  
438 ( $\text{TMF}_{\text{THg}} = 1.3$ ) and a higher biomagnification factor of MMHg ( $\text{TMF}_{\text{MMHg}} = 2.1$ ).  
439 The high proportions of MMHg, exceeding 95% in higher trophic level consumers (UNEP,  
440 2019), as well as the lack of data in the literature regarding primary producers and particularly  
441 pico- and nanoplankton, may explain these differences. The plankton  $\text{TMF}_{\text{MMHg}}$  in our study  
442 showed high values compared to other marine food webs, which also included higher trophic  
443 level organisms (Atwell et al., 1998; Campbell et al., 2005; Al-Reasi et al., 2007; Nfon et al.,  
444 2009; Lavoie et al., 2010, 2013; Cossa et al., 2012; Chouvelon et al., 2018; Harding et al.,  
445 2018; Hilgendorf et al., 2022). Low growth rates, specific to the oligotrophic Mediterranean  
446 Sea, seem to induce higher MMHg biomagnification in planktivorous food webs (Cossa et al.,  
447 2012; Chouvelon et al., 2018). The %MMHg significantly increased between phyto- and  
448 zooplankton groups from a mean of 3% in the  $0.7\text{--}20 \mu\text{m}$  fractions to 23% in the  $>60 \mu\text{m}$   
449 fraction ( $H = 35.8$ ,  $p < 0.0001$ ) (Fig. 2c), highlighting the preferred biomagnification of  
450 MMHg. Inorganic Hg has a lower assimilation efficiency compared to MMHg, while their  
451 efflux rates are similar (Mason et al., 1996; Lawson and Mason, 1998; Lee and Fisher, 2017),  
452 explaining the inverted patterns between food sources and consumers. Inorganic Hg reacts in  
453 the same way as other trace metals (Chen and Folt, 2000; Ho et al., 2007; Chouvelon et al.,  
454 2019; Chifflet et al., 2023). To our knowledge, there is no previous estimation of MMHg  
455 biomagnification in plankton food web considering different size-fractions of phyto- and  
456 zooplankton. The few studies that have explored this point consisted of models for the  
457 Mediterranean Sea (Rosati et al., 2022) and the global ocean (Zhang et al., 2020; Wu et al.,  
458 2021). Without exception, these models indicate bioreduction of MMHg in plankton food

459 webs, mainly composed of herbivorous and omnivorous organisms, and biomagnification  
460 when carnivorous organisms were taken into consideration. Our results suggest the contrary,  
461 biomagnification of MMHg occurs in all plankton consumers, independently of their trophic  
462 position.

463 The trophic transfer efficiency between phytoplankton (0.7–2.7 and 2.7–20  $\mu\text{m}$ ) and  
464 zooplankton size-fractions ( $>60 \mu\text{m}$ ) was assessed by considering the total amounts of THg  
465 and MMHg available in their respective biomasses at the CML (Fig. 4). THg amounts in  
466 phyto- and zooplankton biomass was 15 and 1  $\text{ng m}^{-3}$  of sea water, respectively, while their  
467 respective MMHg contents amounted to 200 and 300  $\text{pg m}^{-3}$ . MMHg is almost 10 times  
468 higher than that modeled in the Mediterranean Sea (Rosati et al., 2022). The trophic transfer  
469 efficiency of THg ranged from 2 to 21% (average 8%), while it was higher for MMHg,  
470 ranging from 11 to 169 %, with an average of 78%. Zooplankton can represent a comparable  
471 or even larger sink of MMHg when compared to phytoplankton. Longer lifespan together  
472 with bioaccumulation can lead to a higher MMHg storage in zooplankton despite their lower  
473 biomass than phytoplankton. The MMHg trophic transfer efficiency estimated here presented  
474 a higher value than the zooplankton daily grazing, which accounted for 2.7 to 27% of the  
475 phytoplankton stock (Fierro-González et al., 2023). Considering daily grazing and Hg  
476 concentrations in phytoplankton and assuming a quantitative assimilation of MMHg,  
477 zooplankton organisms should have grazed for 6 to 13 days to reach the MMHg  
478 concentrations measured in their body. This short integration time suggested that zooplankton  
479 could be a good bioindicator of Hg exposure over days or a few weeks. The results reported  
480 here indicated that MMHg was efficiently biomagnified and transferred along the plankton  
481 food web, in contrast to a rather inefficient transfer of inorganic Hg.

### 482 483 **3.4 Spatial variability of THg and MMHg**

484 Dissolved Hg (dHg) concentrations ranged from 50 to 165  $\text{pg L}^{-1}$  at St11 and St4,  
485 respectively. Dissolved MeHg (dMeHg) concentrations ranged from detection limits (7  $\text{pg L}^{-1}$ )  
486 at St1, St9, St11, St17 and St19 to 26  $\text{pg L}^{-1}$  in St3. Both Hg species were comparable to  
487 previous studies in the Mediterranean Sea (Jiskra et al., 2021; Cossa et al., 2022).

488 THg and MMHg concentrations in phytoplankton (0.7–20  $\mu\text{m}$ ) showed strong spatial  
489 variations in the western Mediterranean, with the highest values in the smallest fraction  
490 recorded at St1 (Toulon in the north) and St17 (Gabès in the south) (Table S3 and S4).

491 Volume concentrations of MMHg in the 0.7 to 20  $\mu\text{m}$  fractions (in  $\text{pg L}^{-1}$ ) were significantly



492 correlated to phytoplankton biomass ( $R^2 = 0.49$ ,  $p < 0.001$ ) (Table S10). This highlighted the  
493 influence of the biomass on Hg-uptake at the basis of the plankton food web. Zones with high  
494 biomass of small phytoplankton cells may store a large amount of Hg in phytoplankton,  
495 bioavailable then for grazers and higher trophic level consumers. In addition, inorganic Hg  
496 may represent a substrate for MMHg production.

497 Our results suggested higher THg and especially MMHg differences in zooplankton between  
498 stations than between size-fractions (Fig. 5, Table S3 and S4). The high growth rates and  
499 short life cycles of zooplankton make it a potentially relevant biomonitor for ambient MMHg  
500 concentrations over short periods, as suggested in the previous section. This observation  
501 contrasts with the high variability reported in marine organisms of higher trophic level related  
502 in particular to longer life span and larger home ranges (UNEP, 2019).

503 THg and MMHg concentrations of zooplankton size-fractions available at all stations (60–  
504 200, 200–500 and \*500–1000  $\mu\text{m}$ , \*unavailable for St17) were pooled to test zooplankton  
505 spatial variability that appeared higher for MMHg than for THg (Fig. 5). Significant  
506 differences were reported between stations only for MMHg ( $H = 24.0$ ,  $p = 0.004$ ). Mean  
507 MMHg concentrations differed ten-fold between minimum ( $0.6 \text{ ng g}^{-1} \text{ dw}$ , St17) and  
508 maximum values ( $9.4 \text{ ng g}^{-1} \text{ dw}$ , St1). This highlighted the importance of measuring MMHg  
509 in consumers with lower trophic levels. Zooplankton from northern (St1, 2, 3 and 4) and  
510 offshore (St9, 10 and 11) areas presented higher MMHg concentrations than those from the  
511 southern area (St15, 17 and 19) ( $H = 14.0$ ,  $p = 0.001$ ). A  $\text{TMF}_{\text{MMHg}} < 1$  indicated a  
512 bioreduction of MMHg in zooplankton and consequently a lower exposure to Hg of  
513 zooplankton along the Tunisian coast (St17 and 19). (Fig. 6).

514 The two axes of the PCA analysis, performed between THg, MMHg, POC, C/N, protein,  
515 lipids,  $\delta^{13}\text{C}$ ,  $\delta^{15}\text{N}$ , and biomass values in zooplankton per station, explained 57% of the  
516 variability (Fig. S2). Two groups of stations were observed along the first axis: the first group  
517 gathering St1, 2, 9, 10 and 11, and the second one including St3, 4, 15, 17, and 19. The first  
518 group was related to high concentrations in POC, proteins, lipids, THg, MMHg, trophic level  
519 and  $\delta^{15}\text{N}$  in zooplankton, while the second group was correlated with high values of C/N,  $\delta^{13}\text{C}$   
520 and zooplankton biomass. MMHg in zooplankton increased with the trophic level ( $\delta^{15}\text{N}$  may  
521 be used as a proxy). Zooplankton MMHg decreased with increasing amounts of organic  
522 matter, likely because of the affinity of POC, proteins and lipids for Hg. MMHg  
523 concentrations in zooplankton were high in oligotrophic, low productivity areas with low  
524 zooplankton biomass, high trophic level and high POC, protein and lipid content. Under



525 oligotrophic conditions, zooplankton were limited by food resources and, as a result, their  
526 biomass and growth rates decreased, and increasing Hg bioaccumulation was observed.  
527 Oligotrophic ecosystems also have longer food webs with intermediate consumers (ciliates,  
528 dinoflagellates, microzooplankton, etc.), which may constitute a trophic link between pico-  
529 and nanoplankton, and mesozooplankton, generating additional food steps and probably  
530 increasing the biomagnification processes (Søreide et al., 2006; Kürten et al., 2013).

531 The negative correlation in zooplankton between MMHg and its biomass may suggest a  
532 biodilution with growth in more productive areas. This is probably the case in the Gulf of  
533 Gabès where lower Hg concentrations in planktivorous species were already reported  
534 compared to those in the north-western Mediterranean basin (Aboul-Dahab et al., 1986; Ben  
535 Hassine et al., 1990; Joiris et al., 1999). Moreover, in ecosystems where nutrients and  
536 phytoplankton resources are abundant, herbivory is the main food pathway, generating lower  
537 trophic level ecosystems (Sommer et al., 2002) and thus potentially lower Hg concentrations  
538 in consumers.

539 Coastal areas have been considered to be hotspots for Hg-accumulation due to proximity to  
540 sediment and resuspension (Chen et al., 2008). Cossa et al. (2018) showed that MeHg  
541 concentrations in subsurface waters are higher in Mediterranean offshore waters. Although  
542 coastal regions are subjected to additional sources of Hg (submarine groundwater discharge,  
543 rivers and sediments), our results evidenced a lower trophic transfer of Hg in plankton food  
544 webs compared to offshore areas, as also observed by Cossa et al. (2012) in the Gulf of Lion.  
545 There is indeed more and more evidence of *in situ* Hg methylation in oxygenated waters of  
546 the open ocean (Mason and Fitzgerald, 1990; Blum et al., 2013; Masbou et al., 2015; Villar et  
547 al. 2020; Liu et al., 2021), and the Mediterranean Sea (Cossa et al. 2022).

548 However, potential sources of Hg in contaminated areas must be considered as well. Toulon  
549 Bay represents an important hotspot of Hg, containing large amounts in its sediments (Tessier  
550 et al., 2011) and may be responsible for the highest concentrations measured in this study.  
551 High concentrations of THg and MMHg have already been recorded in fish and mussels in  
552 Toulon Bay (Cresson et al., 2014; Briant et al., 2017).

#### 554 4. Conclusions

555  
556 Few Hg data are currently available for plankton, particularly for MMHg, and they generally  
557 show wide variations. An inappropriate plankton sampling strategy may lead to the collection

558 of organisms with a heterogenous size and composition, highly impacting their Hg and  
1 559 MMHg concentrations. We have tried to overcome these limitations with a dedicated  
2  
3 560 sampling strategy for the acquisition of different phyto- and zooplankton size-classes, the  
4  
5 561 acquisition of trophic proxies and the collection of sufficient biomass for complementary  
6  
7 562 biological and chemical analyses.

8  
9 563 High THg and MMHg bioconcentration values were observed for phytoplankton, with the  
10  
11 564 highest values for picoplankton. Small phytoplankton cells were the main contributors to  
12  
13 565 primary production in the Mediterranean waters during our sampling campaign and a major  
14  
15 566 food source for zooplankton. Phytoplankton THg concentrations were higher overall  
16  
17 567 compared to the existing literature. Our study implies that phytoplankton in the oligotrophic  
18 568 Mediterranean Sea is an important driver in the biomagnification of MMHg.

19  
20 569 Although THg accumulation through diet is a widely accepted process, our results show that  
21  
22 570 THg bioreduces while MMHg bioaccumulates in the plankton food web. Different kinetics of  
23  
24 571 iHg and MMHg have been evidenced in plankton, supporting the need to analyze both phyto-  
25  
26 572 and zooplankton, and to relate them to their species/group composition in future studies.

27 573 Biomagnification of MMHg in all plankton consumers was evidenced, independently of their  
28  
29 574 trophic position. High biomagnification factors were measured compared to previous studies,  
30  
31 575 suggesting an effective transfer in Mediterranean plankton food webs.

32  
33 576 Moreover, the biochemical composition of zooplankton, particularly the availability of POC,  
34  
35 577 proteins and lipids appears to have an important role in MMHg bioaccumulation.

36 578 Spatial variability in MMHg concentrations in zooplankton was important, with ten-fold  
37  
38 579 differences between areas. Productivity gradients may explain these contrasts. Higher  
39  
40 580 zooplankton MMHg concentrations were measured in low productive areas offshore. In  
41  
42 581 contrast, more productive coastal planktonic food webs showed lower zooplankton MMHg  
43  
44 582 concentrations. Our results suggest a lower impact of Hg on plankton food webs in the less  
45  
46 583 poorly-studied southern Mediterranean Sea, but more observations are needed to corroborate  
47  
48 584 this. Oligotrophy and plankton trophodynamics were key factors in the transfer of Hg in the  
49  
50 585 Mediterranean Sea, playing probably an important role in the Hg transfer along food webs.  
51  
52 586 Our study may thus contribute to explaining the higher Hg levels observed in Mediterranean  
53  
54 587 apex predators. The impact of climate change is thought to contribute to the increase of the  
55  
56 588 oligotrophy and the decrease in size of phytoplankton and may thus exacerbate Hg  
57  
58 589 accumulation in Mediterranean marine food webs in the future. Overall, our study suggests  
59  
60 590 that bioconcentration of MMHg into phytoplankton and subsequent bioaccumulation and

591 biomagnification are by far the most important factors driving higher trophic level MMHg  
1  
2 592 exposure. As such, the efforts in reducing Hg emissions within the Minamata Convention may  
3  
4 593 be outweighed by the effects of climate change on the lower marine food web structure.

5 594  
6  
7  
8  
9  
10  
11  
12  
13  
14  
15  
16  
17  
18  
19  
20  
21  
22  
23  
24  
25  
26  
27  
28  
29  
30  
31  
32  
33  
34  
35  
36  
37  
38  
39  
40  
41  
42  
43  
44  
45  
46  
47  
48  
49  
50  
51  
52  
53  
54  
55  
56  
57  
58  
59  
60  
61  
62  
63  
64  
65

595 **Author contribution statement**

1  
2 596 Conception and design of study: DB, LEHB, FC, MT, JK

3  
4 597 Acquisition of data: JATO, JK, BT, MT, FC

5  
6 598 Analysis and/or interpretation of data: JATO, DB, LEHB, MHV, MT, AD, BT, JK

7  
8 599 Drafting of the manuscript: JATO, DB, LEHB, MHV, MT

9  
10 600 Revising/editing of the manuscript: JATO, DB, LEHB, MHV, AD, MVL, IGA, JK, BT, FC,

11  
12 601 MT

13  
14 602 Project administration and funding acquisition: DB, MT, FC

15  
16 603

17  
18 604 **Acknowledgements**

19  
20 605 The authors wish to thank the crew of the R/V Antea and the various platforms of the

21  
22 606 Mediterranean Institute of Oceanography which have contributed to the data acquisition:

23  
24 607 Plateforme Analytique de Chimie des Environnements Marins (PACEM) for the POC/PON

25  
26 608 measurements, Plateforme Régionale de Cytométrie pour la Microbiologie (PRECYM) for

27  
28 609 cytometric analyses, Microscopie et Imagerie numérique (MIM) for identification expertise

29  
30 610 and the Service Atmosphère-Mer (SAM) for the technical and operational tasks. The authors

31  
32 611 thank the LIENSs joint research unit (CNRS - La Rochelle University) for the measurement

33  
34 612 of  $\delta^{13}\text{C}$  and  $\delta^{15}\text{N}$  values. The MERITE-HIPPOCAMPE project has been funded by the cross-

35  
36 613 disciplinary Pollution & Contaminants axis of the CNRS-INSU MISTRALS program (joint

37  
38 614 action of the MERMEX-MERITE and CHARMEX subprograms) and received support from

39  
40 615 the IRD French-Tunisian International Joint Laboratory (LMI) COSYS-Med. We are grateful

41  
42 616 for the additional funding received from IFREMER, the MIO Action Sud and Transverse

43  
44 617 Axis programs (CONTAM Transversal Axis), and from the IRD Ocean Department. This

45  
46 618 study received funding by the CONTAMPUMP project (ANR JCJC #19-CE34-0001-01). We

47  
48 619 warmly thank Michael Paul for improvement of the English. Finally, we acknowledge two

49  
50 620 reviewers for their helpful and constructive comments and suggestions.

51  
52 621

53  
54 622 **Supplementary information**

55  
56 623 Supplementary material related to this article is available online.

57

58

59

60

61

62

63

64

65

624           **References**

- 1  
2 625 Aboul-Dahab, O., Halim, Y. and ElRayis, O., 1986. Mercury species in coastal marine organisms  
3  
4 626           from different trophic levels west of Alexandria. In FAO/UNEP/WHO/IOC/IAEA  
5 627           Meeting on the biogeochemical cycle of mercury in the Mediterranean. FAO Fish  
6 628           Report. No. 325 (suppl), Rome, pp. 1-7.  
7  
8  
9 629 Al-Reasi, H.A., Ababneh, F.A., Lean, D.R., 2007. Evaluating mercury biomagnification in fish  
10 630           from a tropical marine environment using stable isotopes ( $\delta^{13}\text{C}$  and  $\delta^{15}\text{N}$ ).  
11  
12 631           *Environmental Toxicology and Chemistry* 26, 1572–1581. [https://doi.org/10.1897/06-](https://doi.org/10.1897/06-359R.1)  
13 632           359R.1  
14  
15  
16 633 Aston, S.R., Fowler, S.W., 1985. Mercury in the open Mediterranean: evidence of  
17 634           contamination? *Science of the Total Environment* 43, 13–26.  
18  
19 635           [https://doi.org/10.1016/0048-9697\(85\)90028-2](https://doi.org/10.1016/0048-9697(85)90028-2)  
20  
21  
22 636 Atwell, L., Hobson, K.A., Welch, H.E., 1998. Biomagnification and bioaccumulation of mercury  
23 637           in an arctic marine food web: insights from stable nitrogen isotope analysis. *Canadian*  
24 638           *Journal of Fisheries and Aquatic Sciences*. 55, 1114–1121. [https://doi.org/10.1139/f98-](https://doi.org/10.1139/f98-001)  
25 639           001  
26  
27  
28  
29 640 Bacci, E., 1989. Mercury in the Mediterranean. *Marine Pollution Bulletin* 20, 59–63.  
30  
31 641           [https://doi.org/10.1016/0025-326X\(89\)90227-0](https://doi.org/10.1016/0025-326X(89)90227-0)  
32  
33 642 Baeyens, W., Leermakers, M., Papina, T., Saprykin, A., Brion, N., Noyen, J., De Gieter, M.,  
34 643           Elskens, M., Goeyens, L., 2003. Bioconcentration and biomagnification of mercury and  
35 644           methylmercury in North Sea and Scheldt estuary fish. *Archives of Environmental*  
36 645           *Contamination and Toxicology* 45, 498–508. [https://doi.org/10.1007/s00244-003-2136-](https://doi.org/10.1007/s00244-003-2136-4)  
37 646           4  
38  
39  
40  
41  
42 647 Bănaru, D., Diaz, F., Verley, P., Campbell, R., Navarro, J., Yohia, C., Oliveros-Ramos, R.,  
43 648           Mellon-Duval, C., Shin, Y.-J., 2019. Implementation of an end-to-end model of the Gulf  
44 649           of Lions ecosystem (NW Mediterranean Sea). I. Parameterization, calibration and  
45 650           evaluation. *Ecological Modelling* 401, 1–19.  
46  
47 651           <https://doi.org/10.1016/j.ecolmodel.2019.03.005>  
48  
49  
50  
51 652 Bănaru, D., Mellon-Duval, C., Roos, D., Bigot, J.-L., Souplet, A., Jadaud, A., Beaubrun, P.,  
52 653           Fromentin, J.-M., 2013. Trophic structure in the Gulf of Lions marine ecosystem (north-  
53 654           western Mediterranean Sea) and fishing impacts. *Journal of Marine Systems* 111–112,  
54 655           45–68. <https://doi.org/10.1016/j.jmarsys.2012.09.010>  
55  
56  
57  
58 656 Bargagli, R., Monaci, F., Sanchez-Hernandez, J.C., Cateni, D., 1998. Biomagnification of  
59  
60

- 657 mercury in an Antarctic marine coastal food web. *Marine Ecology Progress Series* 169,  
1 658 65–76. <https://doi.org/10.3354/meps169065>
- 3 659 Bełdowska, M., Kobos, J., 2018. The variability of Hg concentration and composition of marine  
4 660 phytoplankton. *Environmental Science Pollution Research* 25, 30366–30374.  
5 661 <https://doi.org/10.1007/s11356-018-2948-4>
- 7 662 Ben-Hassine, O. K., Raibaut, A., Ben Souissi, J. and Rousset, L., 1990. Morphologie de  
8 663 *Peroderma cylindricum* (Heller, 1865), Copépode parasite de la *Sardina pilchardus*  
9 664 (Walbaum, 1792) et quelques aspects de son écologie dans les eaux côtières tunisiennes.  
10 665 *Annales des Sciences naturelles, Zoologie Paris* 13(11), 9-16.
- 12 666 Bishop, J.K.B., Lam, P.J., Wood, T.J., 2012. Getting good particles: Accurate sampling of  
13 667 particles by large volume in-situ filtration: Getting good particles. *Limnology and*  
14 668 *Oceanography: Methods* 10, 681–710. <https://doi.org/10.4319/lom.2012.10.681>
- 16 669 Blum, J.D., Popp, B.N., Drazen, J.C., Anela Choy, C., Johnson, M.W., 2013. Methylmercury  
17 670 production below the mixed layer in the North Pacific Ocean. *Nature Geosciences* 6,  
18 671 879–884. <https://doi.org/10.1038/ngeo1918>
- 20 672 Boudriga, I., Thyssen, M., Zouari, A., Garcia, N., Tedetti, M., Bel Hassen, M., 2022.  
21 673 Ultraphytoplankton community structure in subsurface waters along a North-South  
22 674 Mediterranean transect. *Marine Pollution Bulletin* 182, 113977.  
23 675 <https://doi.org/10.1016/j.marpolbul.2022.113977>
- 25 676 Briant, N., Chouvelon, T., Martinez, L., Brach-Papa, C., Chiffolleau, J., Savoye, N., Sonke, J.,  
26 677 Knoery, J., 2017. Spatial and temporal distribution of mercury and methylmercury in  
27 678 bivalves from the French coastline. *Marine Pollution Bulletin* 114, 1096–1102.  
28 679 <https://doi.org/10.1016/j.marpolbul.2016.10.018>
- 30 680 Buckman, K.L., Lane, O., Kotnik, J., Bratkic, A., Sprovieri, F., Horvat, M., Pirrone, N., Evers,  
31 681 D.C., Chen, C.Y., 2018. Spatial and taxonomic variation of mercury concentration in  
32 682 low trophic level fauna from the Mediterranean Sea. *Ecotoxicology* 27, 1341–1352.  
33 683 <https://doi.org/10.1007/s10646-018-1986-5>
- 35 684 Campbell, L.M., Norstrom, R.J., Hobson, K.A., Muir, D.C.G., Backus, S., Fisk, A.T., 2005.  
36 685 Mercury and other trace elements in a pelagic Arctic marine food web (Northwater  
37 686 Polynya, Baffin Bay). *Science of The Total Environment* 351–352, 247–263.  
38 687 <https://doi.org/10.1016/j.scitotenv.2005.02.043>
- 40 688 Carlotti, F., Thibault-Botha, D., Nowaczyk, A., Lefèvre, D., 2008. Zooplankton community  
41 689 structure, biomass and role in carbon fluxes during the second half of a phytoplankton

690 bloom in the eastern sector of the Kerguelen Shelf (January–February 2005). *Deep Sea*  
1 691 *Research Part II: Topical Studies in Oceanography* 55, 720–733.  
2  
3 692 <https://doi.org/10.1016/j.dsr2.2007.12.010>  
4  
5 693 Charette, T., Rosabal, M., Amyot, M., 2021. Mapping metal (Hg, As, Se), lipid and protein  
6  
7 694 levels within fish muscular system in two fish species (Striped Bass and Northern Pike).  
8  
9 695 *Chemosphere* 265, 129036. <https://doi.org/10.1016/j.chemosphere.2020.129036>  
10  
11 696 Chen, C.Y., Folt, C.L., 2000. Bioaccumulation and Diminution of Arsenic and Lead in a  
12  
13 697 *Freshwater Food Web. Environmental Science & Technology* 34, 3878–3884.  
14  
15 698 <https://doi.org/10.1021/es991070c>  
16  
17 699 Chen, C., Amirbahman, A., Fisher, N., Harding, G., Lamborg, C., Nacci, D., Taylor, D., 2008.  
18  
19 700 Methylmercury in Marine Ecosystems: Spatial Patterns and Processes of Production,  
20  
21 701 Bioaccumulation, and Biomagnification. *EcoHealth* 5, 399–408.  
22  
23 702 <https://doi.org/10.1007/s10393-008-0201-1>  
24  
25 703 Chifflet, S., Briant, N., Tesán-Onrubia, J.A., Zaaboub, N., Amri, S., Radakovitch, O., Bănaru,  
26  
27 704 D., Tedetti, M., 2023. Distribution and accumulation of trace metal in the planktonic  
28  
29 705 food web of the Mediterranean Sea (MERITE-HIPPOCAMPE campaign). *Marine*  
30  
31 706 *Pollution Bulletin* 186, 114384. <https://doi.org/10.1016/j.marpolbul.2022.114384>.  
32  
33 707 Chouvelon, T., Cresson, P., Bouchouca, M., Brach-Papa, C., Bustamante, P., Crochet, S.,  
34  
35 708 Marco-Miralles, F., Thomas, B., Knoery, J., 2018. Oligotrophy as a major driver of  
36  
37 709 mercury bioaccumulation in medium-to high-trophic level consumers: A marine  
38  
39 710 ecosystem-comparative study. *Environmental Pollution* 233, 844–854.  
40  
41 711 <https://doi.org/10.1016/j.envpol.2017.11.015>  
42  
43 712 Chouvelon, T., Strady, E., Harmelin-Vivien, M., Radakovitch, O., Brach-Papa, C., Crochet, S.,  
44  
45 713 Knoery, J., Rozuel, E., Thomas, B., Tronczynski, J., Chiffolleau, J.-F., 2019. Patterns of  
46  
47 714 trace metal bioaccumulation and trophic transfer in a phytoplankton-zooplankton-small  
48  
49 715 pelagic fish marine food web. *Marine Pollution Bulletin* 146, 1013–1030.  
50  
51 716 <https://doi.org/10.1016/j.marpolbul.2019.07.047>  
52  
53 717 Cinnirella, S., Bruno, D.E., Pirrone, N., Horvat, M., Živković, I., Evers, D.C., Johnson, S.,  
54  
55 718 Sunderland, E.M., 2019. Mercury concentrations in biota in the Mediterranean Sea, a  
56  
57 719 compilation of 40 years of surveys. *Scientific Data* 6, 205.  
58  
59 720 <https://doi.org/10.1038/s41597-019-0219-y>  
60  
61 721 Cossa, D., Martin, J.-M., 1991. Mercury in the Rhône delta and adjacent marine areas. *Marine*  
62  
63 722 *Chemistry, Reactivity of Chemical Species in Aquatic Environments* 36, 291–302.  
64  
65

- 723 [https://doi.org/10.1016/S0304-4203\(09\)90067-6](https://doi.org/10.1016/S0304-4203(09)90067-6)
- 1  
2 724 Cossa, D., Coquery, M., 2005. The Mediterranean Mercury Anomaly, a Geochemical or a  
3  
4 725 Biological Issue, in: Saliot, A. (Ed.), The Mediterranean Sea. Springer Berlin  
5  
6 726 Heidelberg, Berlin, Heidelberg, pp. 177–208. <https://doi.org/10.1007/b107147>
- 7  
8 727 Cossa, D., Averty, B., Pirrone, N., 2009. The origin of methylmercury in open Mediterranean  
9  
10 728 waters. *Limnology and Oceanography* 54, 837–844.  
11  
12 729 <https://doi.org/10.4319/lo.2009.54.3.0837>
- 13  
14 730 Cossa, D., Harmelin-Vivien, M., Mellon-Duval, C., Loizeau, V., Averty, B., Crochet, S., Chou,  
15  
16 731 L., Cadiou, J.-F., 2012. Influences of Bioavailability, Trophic Position, and Growth on  
17  
18 732 Methylmercury in Hakes (*Merluccius merluccius*) from Northwestern Mediterranean  
19  
20 733 and Northeastern Atlantic. *Environmental Science & Technology* 46, 4885–4893.  
21  
22 734 <https://doi.org/10.1021/es204269w>
- 23  
24 735 Cossa, D., Knoery, J., Bănar, D., Harmelin-Vivien, M., Sonke, J.E., Hedgecock, I.M., Bravo,  
25  
26 736 A.G., Rosati, G., Canu, D., Horvat, M., Sprovieri, F., Pirrone, N., Heimbürger-Boavida,  
27  
28 737 L.-E., 2022. Mediterranean Mercury Assessment 2022: An Updated Budget, Health  
29  
30 738 Consequences, and Research Perspectives. *Environmental Science & Technology* 56,  
31  
32 739 3840–3862. <https://doi.org/10.1021/acs.est.1c03044>
- 33  
34 740 Covelli, S., Faganeli, J., Horvat, M., Brambati, A., 2001. Mercury contamination of coastal  
35  
36 741 sediments as the result of long-term cinnabar mining activity (Gulf of Trieste, northern  
37  
38 742 Adriatic sea). *Applied Geochemistry* 16, 541–558.
- 39  
40 743 Cresson, P., Bouchouca, M., Miralles, F., Elleboode, R., Mahé, K., Maruszczak, N., Thebault,  
41  
42 744 H., Cossa, D., 2015. Are red mullet efficient as bio-indicators of mercury  
43  
44 745 contamination? A case study from the French Mediterranean. *Marine Pollution Bulletin*  
45  
46 746 91, 191–199. <https://doi.org/10.1016/j.marpolbul.2014.12.005>
- 47  
48 747 Cresson, P., Fabri, M.C., Bouchouca, M., Brach Papa, C., Chavanon, F., Jadaud, A., Knoery, J.,  
49  
50 748 Miralles, F., Cossa, D., 2014. Mercury in organisms from the Northwestern  
51  
52 749 Mediterranean slope: Importance of food sources. *Science of The Total Environment*  
53  
54 750 497–498, 229–238. <https://doi.org/10.1016/j.scitotenv.2014.07.069>
- 55  
56 751 Décima, M., 2022. Zooplankton trophic structure and ecosystem productivity. *Marine Ecology*  
57  
58 752 Progress Series 692, 23–42. <https://doi.org/10.3354/meps14077>
- 59  
60 753 Di Benedetto, A.P.M., Bittar, V.T., Camargo, P.B., Rezende, C.E., Kehrig, H.A., 2012. Mercury  
61  
62 754 and Nitrogen Isotope in a Marine Species from a Tropical Coastal Food Web. *Archives*  
63  
64 755 of *Environmental Contamination and Toxicology* 62, 264–271.



- 756 <https://doi.org/10.1007/s00244-011-9701-z>
- 1  
2 757 Durrieu de Madron, X., Guieu, C., Sempéré, R., Conan, P., Cossa, D., D’Ortenzio, F., Estournel,  
3  
4 758 C., Gazeau, F., Rabouille, C., Stemmann, L., Bonnet, S., Diaz, F., Koubbi, P.,  
5  
6 759 Radakovitch, O., Babin, M., Baklouti, M., Bancon-Montigny, C., Belviso, S.,  
7  
8 760 Bensoussan, N., Bonsang, B., Bouloubassi, I., Brunet, C., Cadiou, J.-F., Carlotti, F.,  
9  
10 761 Chami, M., Charmasson, S., Charrière, B., Dachs, J., Doxaran, D., Dutay, J.-C., Elbaz-  
11  
12 762 Poulichet, F., Eléaume, M., Eyrolles, F., Fernandez, C., Fowler, S., Francour, P.,  
13  
14 763 Gaertner, J.C., Galzin, R., Gasparini, S., Ghiglione, J.-F., Gonzalez, J.-L., Goyet, C.,  
15  
16 764 Guidi, L., Guizien, K., Heimbürger, L.-E., Jacquet, S.H.M., Jeffrey, W.H., Joux, F., Le  
17  
18 765 Hir, P., Leblanc, K., Lefèvre, D., Lejeusne, C., Lemé, R., Loÿe-Pilot, M.-D., Mallet, M.,  
19  
20 766 Méjanelle, L., Mélin, F., Mellon, C., Mériçot, B., Merle, P.-L., Migon, C., Miller, W.L.,  
21  
22 767 Mortier, L., Mostajir, B., Mousseau, L., Moutin, T., Para, J., Pérez, T., Petrenko, A.,  
23  
24 768 Poggiale, J.-C., Prieur, L., Pujo-Pay, M., Pulido-Villena, Raimbault, P., Rees, A.P.,  
25  
26 769 Ridame, C., Rontani, J.-F., Ruiz Pino, D., Sicre, M.A., Taillandier, V., Tamburini, C.,  
27  
28 770 Tanaka, T., Taupier-Letage, I., Tedetti, M., Testor, P., Thébault, H., Thouvenin, B.,  
29  
30 771 Touratier, F., Tronczynski, J., Ulses, C., Van Wambeke, F., Vantrepotte, V., Vaz, S.,  
31  
32 772 Verney, R., 2011. Marine ecosystems’ responses to climatic and anthropogenic forcings  
33 773 in the Mediterranean. *Progress in Oceanography* 91, 97–166.  
34  
35 774 <https://doi.org/10.1016/j.pocan.2011.02.003>
- 36  
37 775 Fierro-González, P., Pagano, M., Guilloux, L., Makhlof, N., Tedetti, M., Carlotti, F., 2023.  
38 776 Zooplankton biomass, size structure, and associated metabolic fluxes with focus on its  
39 777 roles at the chlorophyll maximum layer during the plankton-contaminant MERITE-  
40 778 HIPPOCAMPE cruise. *Marine Pollution Bulletin* 193, 115056.  
41  
42 779 <https://doi.org/10.1016/j.marpolbul.2023.115056>
- 43  
44 780 Fisher, N.S., 1985. Accumulation of metals by marine picoplankton. *Marine Biology* 87, 137–  
45 781 142. <https://doi.org/10.1007/BF00539421>
- 46  
47 782 Foster, K.L., Stern, G.A., Pazerniuk, M.A., Hickie, B., Walkusz, W., Wang, F., Macdonald,  
48 783 R.W., 2012. Mercury Biomagnification in Marine Zooplankton Food Webs in Hudson  
49 784 Bay. *Environmental Science & Technology* 46, 12952–12959.  
50  
51 785 <https://doi.org/10.1021/es303434p>
- 52  
53 786 Fox, A.L., Trefry, J.H., Trocine, R.P., Dunton, K.H., Lasorsa, B.K., Konar, B., Ashjian, C.J.,  
54 787 Cooper, L.W., 2017. Mercury biomagnification in food webs of the northeastern  
55 788 Chukchi Sea, Alaskan Arctic. *Deep Sea Research Part II: Topical Studies in*

- 789 Oceanography, 144, 63–77. <https://doi.org/10.1016/j.dsr2.2017.04.020>
- 1  
2 790 Gosnell, K.J., Balcom, P.H., Tobias, C.R., Gilhooly III, W.P., Mason, R.P., 2017. Spatial and  
3  
4 791 temporal trophic transfer dynamics of mercury and methylmercury into zooplankton and  
5  
6 792 phytoplankton of Long Island Sound. *Limnology and Oceanography* 62, 1122–1138.  
7  
8 793 <https://doi.org/10.1002/lno.10490>
- 9 794 Gosnell, K.J., Mason, R.P., 2015. Mercury and methylmercury incidence and bioaccumulation in  
10  
11 795 plankton from the central Pacific Ocean. *Marine Chemistry* 177, 772–780.  
12  
13 796 <https://doi.org/10.1016/j.marchem.2015.07.005>
- 14 797 Guidi, L., Stemmann, L., Jackson, G.A., Ibanez, F., Claustre, H., Legendre, L., Picheral, M.,  
15  
16 798 Gorskya, G., 2009. Effects of phytoplankton community on production, size, and export  
17  
18 799 of large aggregates: A world-ocean analysis. *Limnology and Oceanography* 54, 1951–  
19  
20 800 1963. <https://doi.org/10.4319/lo.2009.54.6.1951>
- 21  
22 801 Hammerschmidt, C.R., Finiguerra, M.B., Weller, R.L., Fitzgerald, W.F., 2013. Methylmercury  
23  
24 802 Accumulation in Plankton on the Continental Margin of the Northwest Atlantic Ocean.  
25  
26 803 *Environmental Science & Technology* 47, 3671–3677.  
27  
28 804 <https://doi.org/10.1021/es3048619>
- 29 805 Hammerschmidt, C.R., Fitzgerald, W.F., 2006. Bioaccumulation and Trophic Transfer of  
30  
31 806 Methylmercury in Long Island Sound. *Archives of Environmental Contamination and*  
32  
33 807 *Toxicology* 51, 416–424. <https://doi.org/10.1007/s00244-005-0265-7>
- 34  
35 808 Harding, G., Dalziel, J., Vass, P., 2018. Bioaccumulation of methylmercury within the marine  
36  
37 809 food web of the outer Bay of Fundy, Gulf of Maine. *PLOS ONE* 13, e0197220.  
38  
39 810 <https://doi.org/10.1371/journal.pone.0197220>
- 40 811 Harmelin-Vivien, M., Cossa, D., Crochet, S., Bănar, D., Letourneur, Y., Mellon-Duval, C.,  
41  
42 812 2009. Difference of mercury bioaccumulation in red mullets from the north-western  
43  
44 813 Mediterranean and Black seas. *Marine Pollution Bulletin* 58, 679–685.  
45  
46 814 <https://doi.org/10.1016/j.marpolbul.2009.01.004>
- 47 815 Heimbürger, L.-E., Cossa, D., Marty, J.-C., Migon, C., Averty, B., Dufour, A., Ras, J., 2010.  
48  
49 816 Methyl mercury distributions in relation to the presence of nano- and picophytoplankton  
50  
51 817 in an oceanic water column (Ligurian Sea, North-western Mediterranean). *Geochimica*  
52  
53 818 *et Cosmochimica Acta* 74, 5549–5559. <https://doi.org/10.1016/j.gca.2010.06.036>
- 54  
55 819 Heimbürger, L.-E., Sonke, J.E., Cossa, D., Point, D., Lagane, C., Laffont, L., Galfond, B.T.,  
56  
57 820 Nicolaus, M., Rabe, B., van der Loeff, M.R., 2015. Shallow methylmercury production  
58  
59 821 in the marginal sea ice zone of the central Arctic Ocean. *Scientific Reports* 5.

- 822 <https://doi.org/10.1038/srep10318>
- 1  
2 823 Hilgendorf, I.R., Swanson, H.K., Lewis, C.W., Ehrman, A.D., Power, M., 2022. Mercury  
3  
4 824 biomagnification in benthic, pelagic, and benthopelagic food webs in an Arctic marine  
5  
6 825 ecosystem. *Science of The Total Environment* 841, 156424.  
7  
8 826 <https://doi.org/10.1016/j.scitotenv.2022.156424>
- 9 827 Ho, T.-Y., Wen, L.-S., You, C.-F., Lee, D.-C., 2007. The trace metal composition of size-  
10  
11 828 fractionated plankton in the South China Sea: Biotic versus abiotic sources. *Limnology*  
12  
13 829 *and Oceanography* 52, 1776–1788. <https://doi.org/10.4319/lo.2007.52.5.1776>
- 14  
15 830 Horvat, M., Covelli, S., Faganeli, J., Logar, M., Mandić, V., Rajar, R., Širca, A., Žagar, D., 1999.  
16  
17 831 Mercury in contaminated coastal environments; a case study: the Gulf of Trieste.  
18  
19 832 *Science of the Total Environment* 237, 43–56.
- 20  
21 833 Hunt, B.P.V., Carlotti, F., Donoso, K., Pagano, M., D’Ortenzio, F., Taillandier, V., Conan, P.,  
22  
23 834 2017. Trophic pathways of phytoplankton size classes through the zooplankton food  
24  
25 835 web over the spring transition period in the north-west Mediterranean Sea. *Journal of*  
26  
27 836 *Geophysical Research: Oceans* 122, 6309–6324. <https://doi.org/10.1002/2016JC012658>
- 28  
29 837 Jiskra, M., Heimbürger-Boavida, L.-E., Desgranges, M.-M., Petrova, M.V., Dufour, A., Ferreira-  
30  
31 838 Araujo, B., Masbou, J., Chmeleff, J., Thyssen, M., Point, D., Sonke, J.E., 2021.  
32  
33 839 Mercury stable isotopes constrain atmospheric sources to the ocean. *Nature* 597, 678–  
34  
35 840 682. <https://doi.org/10.1038/s41586-021-03859-8>
- 36  
37 841 Joiris, C.R., Holsbeek, L., Laroussi moatemri, N., 1999. Total and Methylmercury in Sardines  
38  
39 842 *Sardinella aurita* and *Sardina pilchardus* from Tunisia. *Marine Pollution Bulletin* 38,  
40  
41 843 188–192. [https://doi.org/10.1016/S0025-326X\(98\)00171-4](https://doi.org/10.1016/S0025-326X(98)00171-4)
- 42  
43 844 Kehrig, H.A., Palermo, E.F.A., Seixas, T.G., Branco, C.W.C., Moreira, I., Malm, O., 2009.  
44  
45 845 Trophic transfer of methylmercury and trace elements by tropical estuarine seston and  
46  
47 846 plankton. *Estuarine, Coastal and Shelf Science* 85, 36–44.  
48  
49 847 <https://doi.org/10.1016/j.ecss.2009.05.027>
- 50  
51 848 Kucuksezgin, F., Altay, O., Uluturhan, E., Kontas, A., 2001. Trace Metal and Organochlorine  
52  
53 849 Residue Levels in Red Mullet (*Mullus barbatus*) from the Eastern Aegean, Turkey.  
54  
55 850 *Water Research* 35, 2327–2332. [https://doi.org/10.1016/S0043-1354\(00\)00504-2](https://doi.org/10.1016/S0043-1354(00)00504-2)
- 56  
57 851 Kürten, B., Painting, S.J., Struck, U., Polunin, N.V.C., Middelburg, J.J., 2013. Tracking seasonal  
58  
59 852 changes in North Sea zooplankton trophic dynamics using stable isotopes.  
60  
61 853 *Biogeochemistry* 113, 167–187. <https://doi.org/10.1007/s10533-011-9630-y>
- 62  
63 854 Lamborg, C.H., Hammerschmidt, C.R., Bowman, K.L., Swarr, G.J., Munson, K.M., Ohnemus,  
64  
65

855 D.C., Lam, P.J., Heimbürger, L.-E., Rijkenberg, M.J.A., Saito, M.A., 2014. A global  
1 856 ocean inventory of anthropogenic mercury based on water column measurements.  
2  
3 857 Nature 512, 65–68. <https://doi.org/10.1038/nature13563>  
4  
5 858 Lamborg, C.H., Hammerschmidt, C.R., Bowman, K.L., 2016. An examination of the role of  
6  
7 859 particles in oceanic mercury cycling. *Philosophical Transactions of the Royal Society A*  
8  
9 860 374, 20150297. <https://doi.org/10.1098/rsta.2015.0297>  
10  
11 861 Lavoie, R.A., Hebert, C.E., Rail, J.-F., Braune, B.M., Yumvihoze, E., Hill, L.G., Lean, D.R.S.,  
12  
13 862 2010. Trophic structure and mercury distribution in a Gulf of St. Lawrence (Canada)  
14  
15 863 food web using stable isotope analysis. *Science of The Total Environment* 408, 5529–  
16  
17 864 5539. <https://doi.org/10.1016/j.scitotenv.2010.07.053>  
18  
19 865 Lavoie, R.A., Jardine, T.D., Chumchal, M.M., Kidd, K.A., Campbell, L.M., 2013.  
20  
21 866 Biomagnification of Mercury in Aquatic Food Webs: A Worldwide Meta-Analysis.  
22  
23 867 *Environmental Science & Technology*, 47, 13385–13394.  
24  
25 868 <https://doi.org/10.1021/es403103t>  
26  
27 869 Lawson, N.M., Mason, R.P., 1998. Accumulation of mercury in estuarine food chains.  
28  
29 870 *Biogeochemistry* 40, 235–247. <https://doi.org/10.1023/A:1005959211768>  
30  
31 871 Leblanc, K., Quéguiner, B., Diaz, F., Cornet, V., Michel-Rodriguez, M., Durrieu de Madron, X.,  
32  
33 872 Bowler, C., Malviya, S., Thyssen, M., Grégori, G., Rembauville, M., Grosso, O.,  
34  
35 873 Poulain, J., de Vargas, C., Pujo-Pay, M., Conan, P., 2018. Nanoplanktonic diatoms are  
36  
37 874 globally overlooked but play a role in spring blooms and carbon export. *Nature*  
38  
39 875 *Communications* 9, 953. <https://doi.org/10.1038/s41467-018-03376-9>  
40  
41 876 Lee, C.-S., Fisher, N.S., 2016. Methylmercury uptake by diverse marine phytoplankton.  
42  
43 877 *Limnology and Oceanography* 61, 1626–1639. <https://doi.org/10.1002/lno.10318>  
44  
45 878 Lee, C.-S., Fisher, N.S., 2017. Bioaccumulation of methylmercury in a marine copepod.  
46  
47 879 *Environmental Toxicology and Chemistry* 36, 1287–1293.  
48  
49 880 <https://doi.org/10.1002/etc.3660>  
50  
51 881 Liu, M., Zhang, Q., Maavara, T., Liu, S., Wang, X., Raymond, P.A., 2021. Rivers as the largest  
52  
53 882 source of mercury to coastal oceans worldwide. *Nature Geosciences*, 14, 672–677.  
54  
55 883 <https://doi.org/10.1038/s41561-021-00793-2>  
56  
57 884 Loseto, L.L., Stern, G.A., Deibel, D., Connelly, T.L., Prokopowicz, A., Lean, D.R.S., Fortier, L.,  
58  
59 885 Ferguson, S.H., 2008. Linking mercury exposure to habitat and feeding behaviour in  
60  
61 886 Beaufort Sea beluga whales. *Journal of Marine Systems*, 74, 1012–1024.  
62  
63 887 <https://doi.org/10.1016/j.jmarsys.2007.10.004>  
64  
65

- 888 Luengen, A.C., Russell Flegal, A., 2009. Role of phytoplankton in mercury cycling in the San  
1 889 Francisco Bay estuary. *Limnology and Oceanography* 54, 23–40.  
2  
3 890 <https://doi.org/10.4319/lo.2009.54.1.0023>  
4
- 5 891 Masbou, J., Point, D., Guillou, G., Sonke, J.E., Lebreton, B., Richard, P., 2015. Carbon Stable  
6  
7 892 Isotope Analysis of Methylmercury Toxin in Biological Materials by Gas  
8  
9 893 Chromatography Isotope Ratio Mass Spectrometry. *Analytical Chemistry* 87, 11732–  
10  
11 894 11738. <https://doi.org/10.1021/acs.analchem.5b02918>
- 12 895 Mason, R.P., Fitzgerald, W.F., 1990. Alkylmercury species in the equatorial Pacific. *Nature* 347,  
13  
14 896 457–459. <https://doi.org/10.1038/347457a0>
- 15  
16 897 Mason, R.P., Reinfelder, J.R., Morel, F.M.M., 1996. Uptake, Toxicity, and Trophic Transfer of  
17  
18 898 Mercury in a Coastal Diatom. *Environmental Science & Technology* 30, 1835–1845.  
19  
20 899 <https://doi.org/10.1021/es950373d>
- 21  
22 900 Mason, R.P., 2021. Coastal Phytoplankton and Mercury Dynamics in Watersheds Along the U.S.  
23  
24 901 East Coast From New Jersey to Maine Assessed Using Particulate and Dissolved  
25  
26 902 Samples Collected in 2015 and 2016. Biological and Chemical Oceanography Data  
27  
28 903 Management Office (BCO-DMO).
- 29 904 Mason, R.P., Buckman, K.L., Seelen, E.A., Taylor, V.F., Chen, C.Y., 2023. An examination of  
30  
31 905 the factors influencing the bioaccumulation of methylmercury at the base of the  
32  
33 906 estuarine food web. *Science of The Total Environment* 886, 163996.  
34  
35 907 <https://doi.org/10.1016/j.scitotenv.2023.163996>
- 36 908 Maulvault, A.L., Custódio, A., Anacleto, P., Repolho, T., Pousão, P., Nunes, M.L., Diniz, M.,  
37  
38 909 Rosa, R., Marques, A., 2016. Bioaccumulation and elimination of mercury in juvenile  
39  
40 910 seabass (*Dicentrarchus labrax*) in a warmer environment. *Environmental Research* 149,  
41  
42 911 77–85. <https://doi.org/10.1016/j.envres.2016.04.035>
- 43  
44 912 Médieu, A., Point, D., Itai, T., Angot, H., Buchanan, P.J., Allain, V., Fuller, L., Griffiths, S.,  
45  
46 913 Gillikin, D.P., Sonke, J.E., Heimbürger-Boavida, L.-E., Desgranges, M.-M., Menkes,  
47  
48 914 C.E., Madigan, D.J., Brosset, P., Gauthier, O., Tagliabue, A., Bopp, L., Verheyden, A.,  
49  
50 915 Lorrain, A., 2022. Evidence that Pacific tuna mercury levels are driven by marine  
51  
52 916 methylmercury production and anthropogenic inputs. *Proceedings of the National*  
53  
54 917 *Academy of Sciences* 119, e2113032119. <https://doi.org/10.1073/pnas.2113032119>
- 55 918 Monperrus, M., Tessier, E., Amouroux, D., Leynaert, A., Huonnic, P., Donard, O.F.X., 2007.  
56  
57 919 Mercury methylation, demethylation and reduction rates in coastal and marine surface  
58  
59 920 waters of the Mediterranean Sea. *Marine Chemistry* 107, 49–63.

- 921 <https://doi.org/10.1016/j.marchem.2007.01.018>
- 1  
2 922 Morel, F.M.M., Kraepiel, A.M.L., Amyot, M., 1998. The Chemical Cycle and Bioaccumulation  
3  
4 923 of Mercury. *Annual Review of Ecology and Systematics* 29, 543–566.  
5  
6 924 <https://doi.org/10.1146/annurev.ecolsys.29.1.543>
- 7 925 Nfon, E., Cousins, I.T., Järvinen, O., Mukherjee, A.B., Verta, M., Broman, D., 2009.  
8  
9 926 Trophodynamics of mercury and other trace elements in a pelagic food chain from the  
10  
11 927 Baltic Sea. *Science of The Total Environment* 407, 6267–6274.  
12  
13 928 <https://doi.org/10.1016/j.scitotenv.2009.08.032>
- 14 929 Outridge, P.M., Mason, R.P., Wang, F., Guerrero, S., Heimbürger-Boavida, L.E., 2018. Updated  
15  
16 930 Global and Oceanic Mercury Budgets for the United Nations Global Mercury  
17  
18 931 Assessment 2018. *Environmental Science & Technology* 52, 11466–11477.  
19  
20 932 <https://doi.org/10.1021/acs.est.8b01246>
- 21  
22 933 Petrova, M.V., Ourgaud, M., Boavida, J.R.H., Dufour, A., Tesán Onrubia, J.A., Lozingot, A.,  
23  
24 934 Heimbürger-Boavida, L.-E., 2020. Human mercury exposure levels and fish  
25  
26 935 consumption at the French Riviera. *Chemosphere* 258, 127232.  
27  
28 936 <https://doi.org/10.1016/j.chemosphere.2020.127232>
- 29 937 Pućko, M., Burt, A., Walkusz, W., Wang, F., Macdonald, R.W., Rysgaard, S., Barber, D.G.,  
30  
31 938 Tremblay, J.-é., Stern, G.A., 2014. Transformation of Mercury at the Bottom of the  
32  
33 939 Arctic Food Web: An Overlooked Puzzle in the Mercury Exposure Narrative.  
34  
35 940 *Environmental Science & Technology* 48, 7280–7288.  
36  
37 941 <https://doi.org/10.1021/es404851b>
- 38 942 Rau, G., Teyssie, J., Rassoulzadegan, F., Fowler, S., 1990. C-13/C-12 and N-15/N-14 variations  
39  
40 943 among size-fractionated marine particles - implications for their origin and trophic  
41  
42 944 relationships. *Marine Ecology Progress Series* 7.
- 43  
44 945 Ravichandran, M., 2004. Interactions between mercury and dissolved organic matter—a review.  
45  
46 946 *Chemosphere* 55, 319–331. <https://doi.org/10.1016/j.chemosphere.2003.11.011>
- 47 947 R Core Team, 2013. R: A Language and Environment for Statistical Computing. R Foundation  
48  
49 948 for Statistical Computing, Vienna.
- 50  
51 949 Remen, M., Nederlof, M.A.J., Folkedal, O., Thorsheim, G., Sitjà-Bobadilla, A., Pérez-Sánchez,  
52  
53 950 J., Oppedal, F., Olsen, R.E., 2015. Effect of temperature on the metabolism, behaviour  
54  
55 951 and oxygen requirements of *Sparus aurata*. *Aquaculture Environment Interactions* 7,  
56  
57 952 115–123. <https://doi.org/10.3354/aei00141>
- 58 953 Rolff, C., 2000. Seasonal variation in  $\delta^{13}\text{C}$  and  $\delta^{15}\text{N}$  of size-fractionated plankton at a coastal  
59  
60  
61  
62  
63  
64  
65

- 954 station in the northern Baltic proper. *Marine Ecology Progress Series* 203, 47–65.  
1 955 <https://doi.org/10.3354/meps203047>  
2  
3 956 Rosati, G., Solidoro, C., Canu, D., 2020. Mercury dynamics in a changing coastal area over  
4  
5 957 industrial and postindustrial phases: Lessons from the Venice Lagoon. *Science of The*  
6  
7 958 *Total Environment* 743, 140586. <https://doi.org/10.1016/j.scitotenv.2020.140586>  
8  
9 959 Rosati, G., Canu, D., Lazzari, P., Solidoro, C., 2022. Assessing the spatial and temporal  
10  
11 960 variability of methylmercury biogeochemistry and bioaccumulation in the  
12  
13 961 Mediterranean Sea with a coupled 3D model. *Biogeosciences* 19, 3663–3682.  
14  
15 962 <https://doi.org/10.5194/bg-19-3663-2022>  
16  
17 963 Schartup, A.T., Qureshi, A., Dassuncao, C., Thackray, C.P., Harding, G., Sunderland, E.M.,  
18  
19 964 2018. A Model for Methylmercury Uptake and Trophic Transfer by Marine Plankton.  
20  
21 965 *Environmental Science & Technology* 52, 654–662.  
22  
23 966 <https://doi.org/10.1021/acs.est.7b03821>  
24  
25 967 Sharif, A., Monperrus, M., Tessier, E., Amouroux, D., 2013. Determination of methyl mercury  
26  
27 968 and inorganic mercury in natural waters at the pgL–1 level: Intercomparison between  
28  
29 969 PT-GC-Pyr-AFS and GC-ICP-MS using Ethylation or Propylation derivatization. *E3S*  
30  
31 970 *Web of Conferences* 1, 09001. <https://doi.org/10.1051/e3sconf/20130109001>  
32  
33 971 Silva, A., Carrera, P., Massé, J., Uriarte, A., Santos, M.B., Oliveira, P.B., Soares, E., Porteiro, C.,  
34  
35 972 Stratoudakis, Y., 2008. Geographic variability of sardine growth across the northeastern  
36  
37 973 Atlantic and the Mediterranean Sea. *Fisheries Research* 90, 56–69.  
38  
39 974 <https://doi.org/10.1016/j.fishres.2007.09.011>  
40  
41 975 Sommer, U., Stibor, H., Katechakis, A., Sommer, F., Hansen, T., 2002. Pelagic food web  
42  
43 976 configurations at different levels of nutrient richness and their implications for the ratio  
44  
45 977 fish production:primary production, in: Vadstein, O., Olsen, Y. (Eds.), *Sustainable*  
46  
47 978 *Increase of Marine Harvesting: Fundamental Mechanisms and New Concepts*. Springer  
48  
49 979 Netherlands, Dordrecht, pp. 11–20. [https://doi.org/10.1007/978-94-017-3190-4\\_2](https://doi.org/10.1007/978-94-017-3190-4_2)  
50  
51 980 Søreide, J.E., Hop, H., Carroll, M.L., Falk-Petersen, S., Hegseth, E.N., 2006. Seasonal food web  
52  
53 981 structures and sympagic–pelagic coupling in the European Arctic revealed by stable  
54  
55 982 isotopes and a two-source food web model. *Progress in Oceanography* 71, 59–87.  
56  
57 983 <https://doi.org/10.1016/j.pocean.2006.06.001>  
58  
59 984 Stern, G.A., Macdonald, R.W., 2005. Biogeographic Provinces of Total and Methyl Mercury in  
60  
61 985 Zooplankton and Fish from the Beaufort and Chukchi Seas: Results from the SHEBA  
62  
63 986 Drift. *Environmental Science & Technology* 39, 4707–4713.  
64  
65

- 987 <https://doi.org/10.1021/es0482278>
- 1  
2 988 Storelli, M.M., Marcotrigiano, G.O., 2001. Total mercury levels in muscle tissue of swordfish  
3 989 (*Xiphias gladius*) and bluefin tuna (*Thunnus thynnus*) from the Mediterranean Sea  
4  
5 990 (Italy). *Journal of Food Protection* 64, 1058–1061. <https://doi.org/10.4315/0362-028x->  
6  
7 991 64.7.1058
- 8  
9 992 Sunderland, E.M., Krabbenhoft, D.P., Moreau, J.W., Strode, S.A., Landing, W.M., 2009.  
10  
11 993 Mercury sources, distribution, and bioavailability in the North Pacific Ocean: Insights  
12  
13 994 from data and models. *Global Biogeochemical Cycles* 23.  
14  
15 995 <https://doi.org/10.1029/2008GB003425>
- 16 996 Tedetti, M., Tronczynski, J., 2019. HIPPOCAMPE Cruise. RV Antea. [https://doi.org/](https://doi.org/10.17600/18000900)  
17  
18 997 10.17600/18000900.
- 19  
20 998 Tedetti, M., Tronczynski, J., Carlotti, F., Pagano, M., Ismail, S.B., Sammari, C., Hassen, M.B.,  
21  
22 999 Desboeufs, K., Poindron, C., Chifflet, S., Zouari, A.B., Abdennadher, M., Amri, S.,  
23  
24 1000 Bănaru, D., Abdallah, L.B., Bhairy, N., Boudriga, I., Bourin, A., Brach-Papa, C., Briant,  
25  
26 1001 N., Cabrol, L., Chevalier, C., Chouba, L., Coudray, S., Yahia, M.N.D., de Garidel-  
27  
28 1002 Thoron, T., Dufour, A., Dutay, J.-C., Espinasse, B., Fierro-González, P., Fournier, M.,  
29  
30 1003 Garcia, N., Giner, F., Guigue, C., Guilloux, L., Hamza, A., Heimbürger-Boavida, L.-E.,  
31  
32 1004 Jacquet, S., Knoery, J., Lajnef, R., Belkahia, N.M., Malengros, D., Martinot, P.L.,  
33  
34 1005 Bosse, A., Mazur, J.-C., Meddeb, M., Misson, B., Pringault, O., Quéméneur, M.,  
35  
36 1006 Radakovitch, O., Raimbault, P., Ravel, C., Rossi, V., Rwawi, C., Hlaili, A.S., Tesán-  
37  
38 1007 Onrubia, J.A., Thomas, B., Thyssen, M., Zaaboub, N., Garnier, C., 2023. Contamination  
39  
40 1008 of planktonic food webs in the Mediterranean Sea: Setting the frame for the MERITE-  
41  
42 1009 HIPPOCAMPE oceanographic cruise (spring 2019). *Marine Pollution Bulletin* 189,  
43  
44 1010 114765. <https://doi.org/10.1016/j.marpolbul.2023.114765>
- 45  
46 1011 Tesán-Onrubia, J.A., Petrova, M.V., Puigcorbó, V., Black, E.E., Valk, O., Dufour, A., Hamelin,  
47  
48 1012 B., Buesseler, K.O., Masqué, P., Le Moigne, F.A.C., Sonke, J.E., Rutgers van der Loeff,  
49  
50 1013 M., Heimbürger-Boavida, L.-E., 2020. Mercury Export Flux in the Arctic Ocean  
51  
52 1014 Estimated from 234 Th/ 238 U Disequilibria. *ACS Earth and Space Chemistry*.  
53  
54 1015 <https://doi.org/10.1021/acsearthspacechem.0c00055>
- 55  
56 1016 Tesán-Onrubia, J.A., Tedetti, M., Carlotti, F., Tenaille, M., Guilloux, L., Pagano, M., Lebreton,  
57  
58 1017 B., Guillou, G., Fierro-González, P., Guigue, C., Chifflet, S., Garcia, T., Boudriga, I.,  
59  
60 1018 Belhassen, M., Zouari, A.B., Bănaru, D., 2023. Spatial variations of biochemical  
61  
62 1019 content and stable isotope ratios of size-fractionated plankton in the Mediterranean Sea



- 1020 (MERITE-HIPPOCAMPE campaign). *Marine Pollution Bulletin* 189, 114787.  
1  
2 1021 <https://doi.org/10.1016/j.marpolbul.2023.114787>
- 3  
4 1022 Tessier, E., Garnier, C., Mullot, J.-U., Lenoble, V., Arnaud, M., Raynaud, M., Mounier, S., 2011.  
5  
6 1023 Study of the spatial and historical distribution of sediment inorganic contamination in  
7  
8 1024 the Toulon bay (France). *Marine Pollution Bulletin* 62, 2075–2086.  
9  
10 1025 <https://doi.org/10.1016/j.marpolbul.2011.07.022>
- 11 1026 Tseng, C.-M., Ang, S.-J., Chen, Y.-S., Shiao, J.-C., Lamborg, C.H., He, X., Reinfelder, J.R.,  
12  
13 1027 2021. Bluefin tuna reveal global patterns of mercury pollution and bioavailability in the  
14  
15 1028 world's oceans. *Proceedings of the National Academy of Sciences* 118.  
16  
17 1029 <https://doi.org/10.1073/pnas.2111205118>
- 18 1030 Tsui, M.T.K., Wang, W.-X., 2004. Uptake and elimination routes of inorganic mercury and  
19  
20 1031 methylmercury in *Daphnia magna*. *Environmental Science & Technology* 38, 808–816.  
21  
22 1032 <https://doi.org/10.1021/es034638x>
- 23  
24 1033 UN-Environment. Global Mercury Assessment 2018. United Nation Environmental Programme,  
25  
26 1034 Chemicals and Health Branch, Programme Chemicals and Health Branch Geneva  
27  
28 1035 Switzerland, 2019; [www.unenvironment.org/resources/publication/global-](http://www.unenvironment.org/resources/publication/global-mercuryassessment-2018)  
29  
30 1036 [mercuryassessment-2018](http://www.unenvironment.org/resources/publication/global-mercuryassessment-2018).
- 31 1037 Villar, E., Cabrol, L., Heimbürger-Boavida, L.-E., 2020. Widespread microbial mercury  
32  
33 1038 methylation genes in the global ocean. *Environmental Microbiology Reports* 12, 277–  
34  
35 1039 287. <https://doi.org/10.1111/1758-2229.12829>
- 36  
37 1040 Wang, F., Outridge, P.M., Feng, X., Meng, B., Heimbürger-Boavida, L.-E., Mason, R.P., 2019.  
38  
39 1041 How closely do mercury trends in fish and other aquatic wildlife track those in the  
40  
41 1042 atmosphere? – Implications for evaluating the effectiveness of the Minamata  
42  
43 1043 Convention. *Science of The Total Environment* 674, 58–70.  
44  
45 1044 <https://doi.org/10.1016/j.scitotenv.2019.04.101>
- 46  
47 1045 Wu, P., Dutkiewicz, S., Monier, E., Zhang, Y., 2021. Bottom-Heavy Trophic Pyramids Impair  
48  
49 1046 Methylmercury Biomagnification in the Marine Plankton Ecosystems. *Environmental*  
50  
51 1047 *Science & Technology*. 55, 15476–15483. <https://doi.org/10.1021/acs.est.1c04083>
- 52  
53 1048 Wu, Y., Wang, W.-X., 2011. Accumulation, subcellular distribution and toxicity of inorganic  
54  
55 1049 mercury and methylmercury in marine phytoplankton. *Environmental Pollution,*  
56  
57 1050 *Nitrogen Deposition, Critical Loads and Biodiversity* 159, 3097–3105.  
58  
59 1051 <https://doi.org/10.1016/j.envpol.2011.04.012>
- 60  
61 1052 Yoon, S.-J., Diener, L.M., Bloom, P.R., Nater, E.A., Bleam, W.F., 2005. X-ray absorption

1053 studies of CH<sub>3</sub>Hg<sup>+</sup>-binding sites in humic substances. *Geochimica et Cosmochimica*  
1 1054 *Acta* 69, 1111–1121. <https://doi.org/10.1016/j.gca.2004.07.036>  
2  
3 1055 Zhang, Y., Jaeglé L., Thompson L., 2014. Natural biogeochemical cycle of mercury in a global  
4  
5 1056 three-dimensional ocean tracer model. *Global Biogeochemical Cycles* 28, 553–570.  
6  
7 1057 <https://doi.org/10.1002/2014GB004814>  
8  
9 1058 Zhang, Y., Soerensen, A.L., Schartup, A.T., Sunderland, E.M., 2020. A global model for  
10  
11 1059 methylmercury formation and uptake at the base of marine food webs. *Global*  
12  
13 1060 *Biogeochemical Cycles*. <https://doi.org/10.1029/2019GB006348>  
14  
15 1061  
16  
17 1062  
18  
19 1063  
20  
21 1064  
22  
23 1065  
24  
25 1066  
26  
27 1067  
28  
29 1068  
30  
31 1069  
32  
33 1070  
34  
35 1071  
36  
37 1072  
38  
39 1073  
40  
41 1074  
42  
43 1075  
44  
45 1076  
46  
47 1077  
48  
49 1078  
50  
51 1079  
52  
53 1080  
54  
55 1081  
56  
57 1082  
58  
59 1083  
60  
61  
62  
63  
64  
65

1084 **Figure captions**

1  
2 1085

3 1086 **Figure 1:** Location of the ten sampling stations of the MERITE-HIPPOCAMPE cruise in the Mediterranean Sea  
4  
5 1087 (April-Mai 2019).

6 1088

7  
8 1089 **Figure 2:** Boxplot of the concentrations of A) THg, B) MMHg (ng g<sup>-1</sup> dw) and C) %MMHg in the different  
9 1090 plankton size-fractions (fractions between 0.7 and 20 μm (green scale) and >60 μm (red scale) for all stations  
10  
11 1091 combined. H = Kruskal–Wallis nonparametric test and the associated p-value for the respective Hg species (H =  
12 1092 24, p < 0.0001; H = 36, p < 0.0001 and H = 30, p < 0.0001, respectively). The mean and median values are  
13  
14 1093 represented by a cross and a horizontal line, respectively, and the box length is defined as the interquartile range.  
15 1094 The minimum and maximum values are represented by whiskers. Mean values with different post-hoc letters are  
16  
17 1095 significantly different (p < 0.05).

18 1096

19  
20 1097 **Figure 3:** Logarithm of THg (A) and MMHg (B) concentrations in function of δ<sup>15</sup>N (‰) in the different phyto-  
21 1098 (green dots) and zooplankton (red dots) size-fractions. The linear regression curve with its equation and the R-  
22  
23 1099 square are indicated.

24 1100

25  
26 1101 **Figure 4:** Transfer efficiency between phytoplankton (0.7 to 20 μm fractions) and zooplankton (>60 μm  
27 1102 fractions) amounts of THg (A) and MMHg (B) (in pg m<sup>-3</sup>) by station. Yellow, orange and red isolines represent  
28  
29 1103 transfer efficiencies of 1, 5 and 10% for THg and 10, 50 and 100% for MMHg, respectively.

30 1104

31  
32 1105 **Figure 5:** Box plots of A) THg (yellow) and B) MMHg (red) (in ng g<sup>-1</sup> dw) concentrations measured in the 60 to  
33 1106 1000 μm zooplankton size-fractions by station. The mean and median values are represented by a cross and a  
34  
35 1107 horizontal line, respectively, and the box length is defined as the interquartile range.

36 1108

37  
38 1109 **Figure 6:** Trophic magnification factors of THg (TMF<sub>THg</sub>, in yellow) and MMHg (TMF<sub>MMHg</sub> in red) at the  
39  
40 1110 different stations. >1 values indicated biomagnification, while <1 indicated bioreduction.

41 1111

42  
43 1112

44 1113

45

46

47

48

49

50

51

52

53

54

55

56

57

58

59

60

61

62

63

64

65

1114 **Figures**

1 1115

2

3

4

5

6

7

8

9

10

11

12

13

14

15

16

17

18

19

20

21

22

23

24

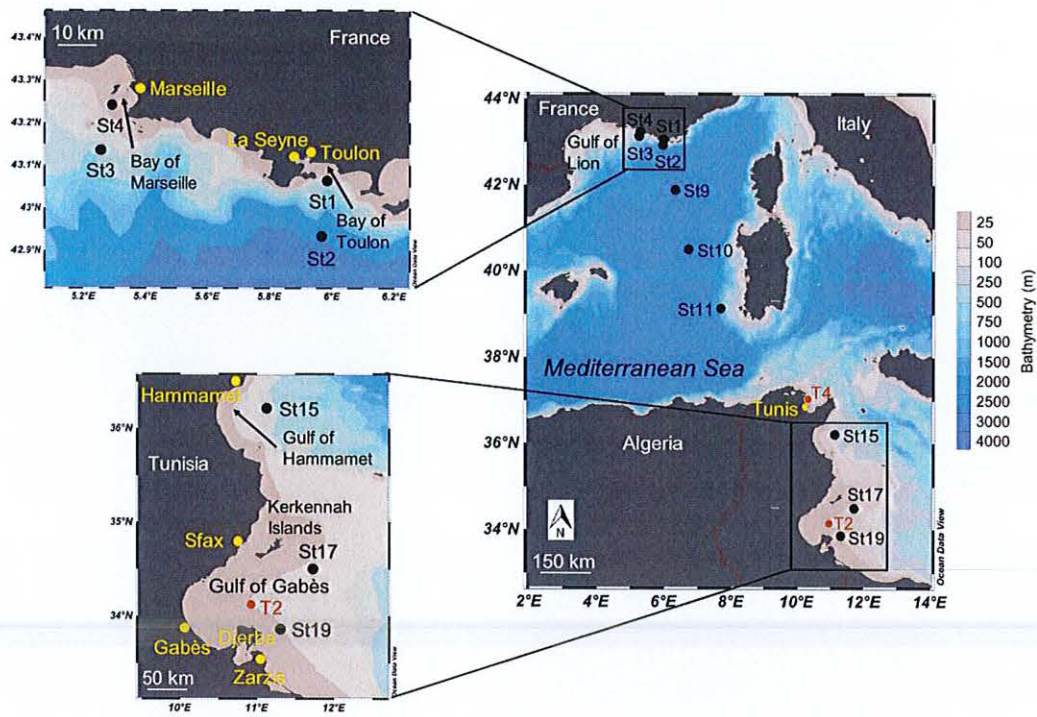
25

26

27 1116

28 1117

**Figure 1**



30

31

32

33

34

35

36

37

38

39

40

41

42

43

44

45

46

47

48

49

50

51

52

53

54

55

56

57

58

59

60

61

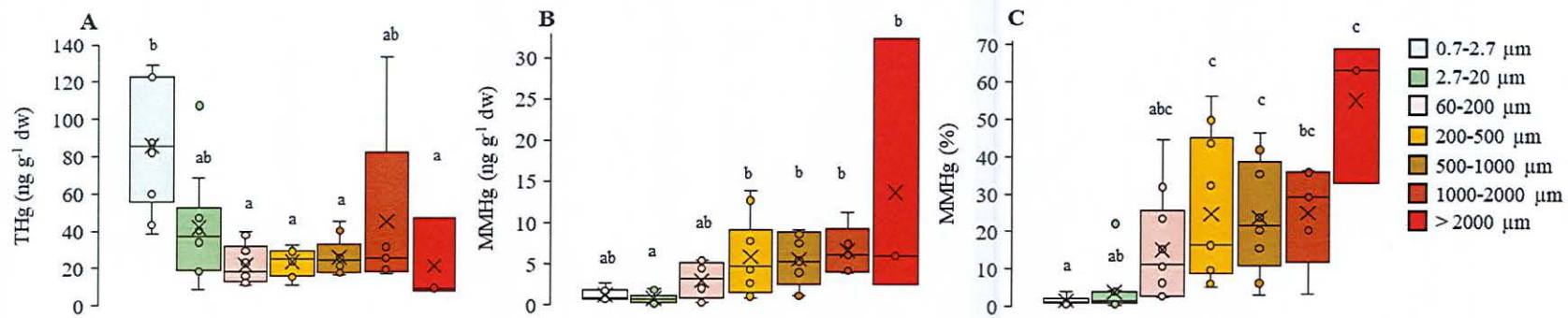
62

63

64

65

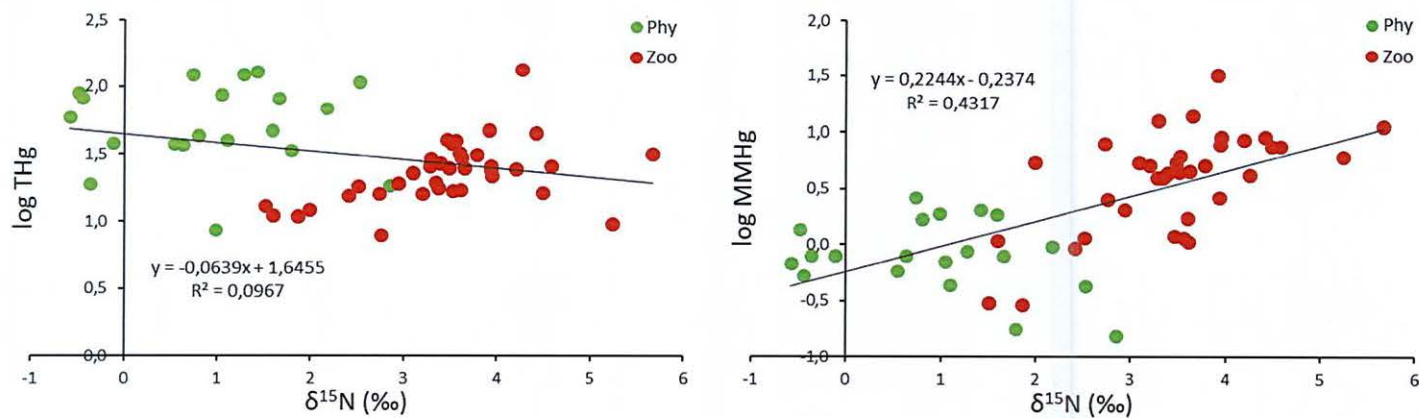
15  
16  
17  
18  
19  
20  
21  
22 1118



35 1119  
36 1120

Figure 2

37 1121  
38 1122  
39 1123  
40 1124  
41 1125  
42  
43  
44



59 1126

60  
61  
62  
63  
64  
65

15  
 16  
 17  
 18  
 19  
 20  
 21  
 22  
 23  
 24  
 25  
 26  
 27  
 28  
 29  
 30  
 31  
 32  
 33  
 34  
 35  
 36  
 37  
 38  
 39  
 40  
 41  
 42  
 43  
 44  
 45  
 46  
 47  
 48  
 49  
 50  
 51  
 52  
 53  
 54  
 55  
 56  
 57  
 58  
 59  
 60  
 61  
 62  
 63  
 64  
 65

Figure 3

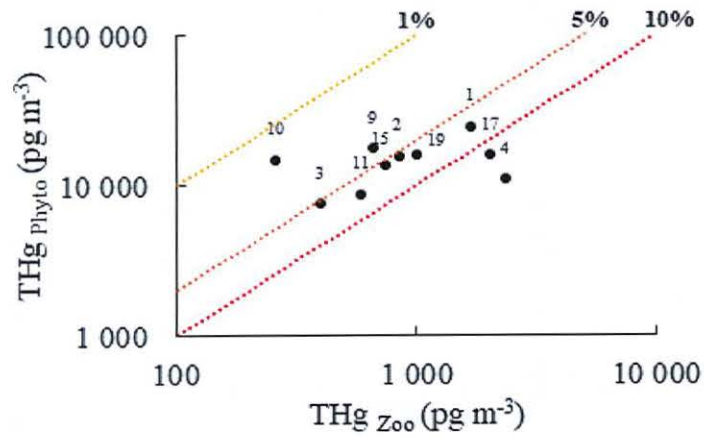
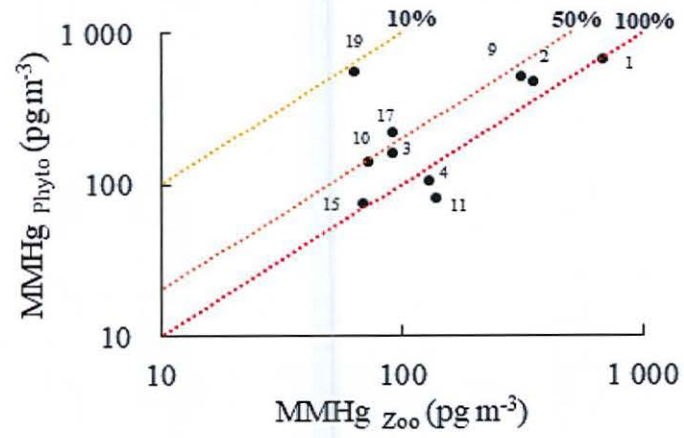


Figure 4



15  
16  
17  
18  
19  
20  
21  
22  
23  
24  
25  
26  
27  
28  
29  
30  
31  
32  
33  
34  
35  
36  
37  
38  
39  
40  
41  
42  
43  
44  
45  
46  
47  
48  
49  
50  
51  
52  
53  
54  
55  
56  
57  
58  
59  
60  
61  
62  
63  
64  
65

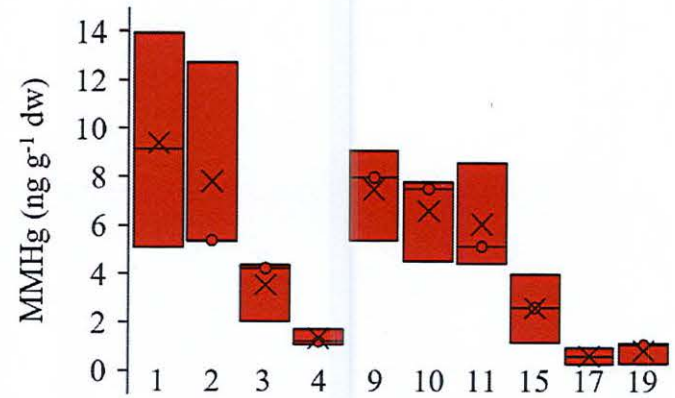
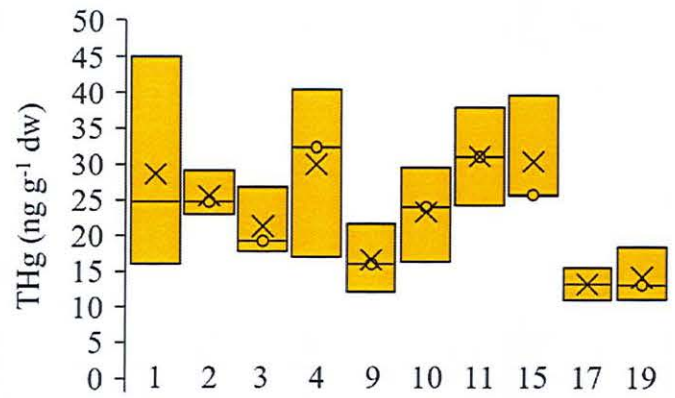
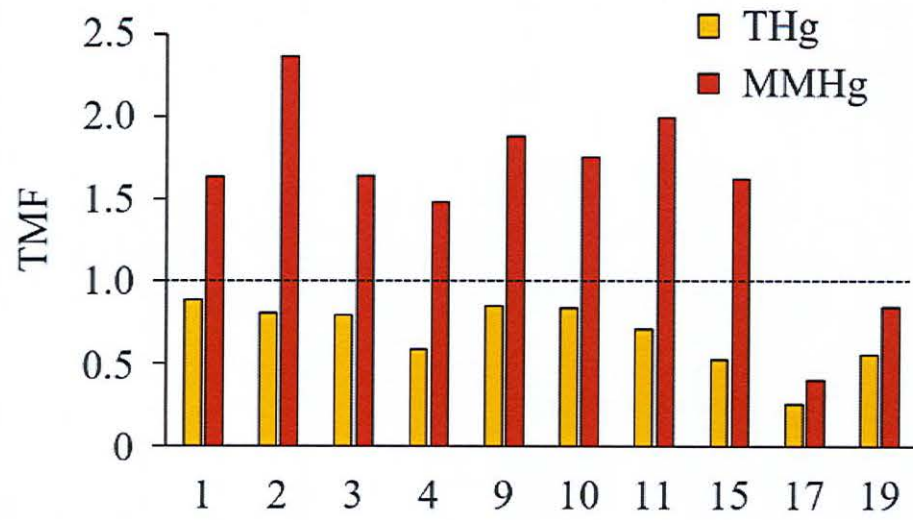


Figure 5

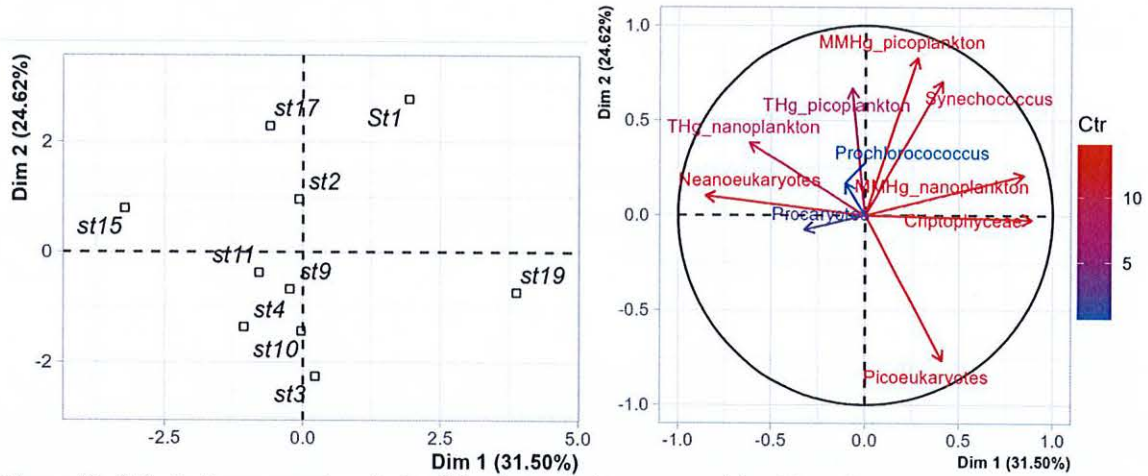
15  
16  
17  
18  
19  
20  
21  
22  
23  
24  
25  
26  
27  
28  
29  
30  
31  
32  
33  
34  
35  
36  
37  
38  
39  
40  
41  
42  
43  
44  
45  
46  
47  
48  
49  
50  
51  
52  
53  
54  
55  
56  
57  
58  
59  
60  
61  
62  
63  
64  
65



1143  
1144 Figure 6



1145 Supplementary information



1146  
 1147 **Figure S1:** Principal component analysis of the phytoplankton composition (*Synechococcus* spp.,  
 1148 *Prochlorococcus* spp., picoeukaryotes, nanoeukaryotes and cryptophyceae), THg and MMHg in the 0.7–2.7 and  
 1149 2.7–20  $\mu\text{m}$  size-fractions by station. Color gradient indicates the contribution of the variables from blue for low  
 1150 contribution to red for high contribution.

1  
 2  
 3  
 4  
 5  
 6  
 7  
 8  
 9  
 10  
 11  
 12  
 13  
 14  
 15  
 16  
 17  
 18  
 19  
 20  
 21  
 22  
 23  
 24  
 25  
 26  
 27  
 28  
 29  
 30  
 31  
 32  
 33  
 34  
 35  
 36  
 37  
 38  
 39  
 40  
 41  
 42  
 43  
 44  
 45  
 46  
 47  
 48  
 49  
 50  
 51  
 52  
 53  
 54  
 55  
 56  
 57  
 58  
 59  
 60  
 61  
 62  
 63  
 64  
 65

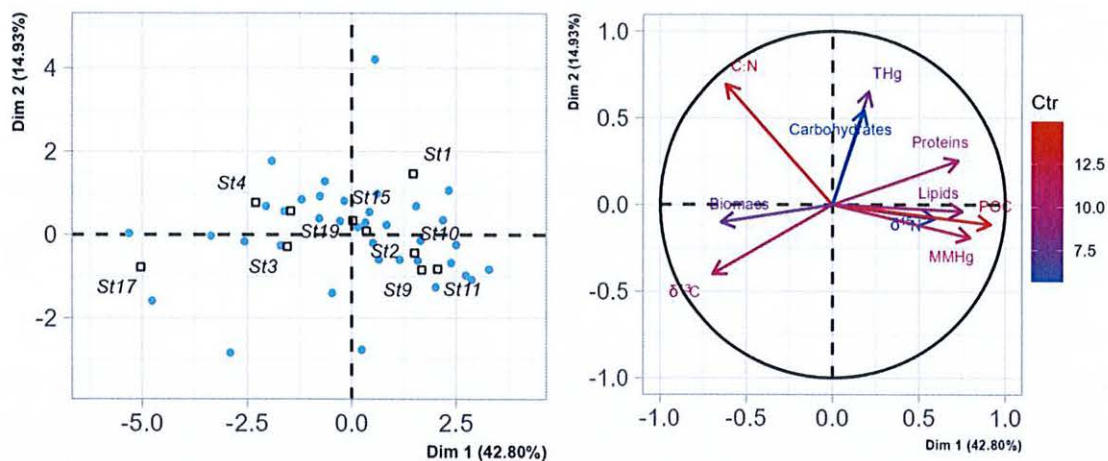


**Figure S2:** Principal component analysis of the biochemical variables (zooplankton biomass,  $\delta^{13}C$ ,  $\delta^{15}N$ , C/N, POC, proteins, carbohydrates and lipids), THg and MMHg in zooplankton (60 to 1000  $\mu m$  fractions) by station. Color gradient indicates the contribution of the variables from blue for low contribution to red for high contribution.

15  
16  
17  
18  
19  
20  
21  
22  
23  
24  
25  
26  
27  
28  
29  
30  
31  
32  
33  
34  
35  
36  
37  
38  
39  
40  
41  
42  
43  
44  
45  
46  
47  
48  
49  
50  
51  
52  
53  
54  
55  
56  
57  
58  
59  
60  
61  
62  
63  
64  
65

**Table S1.** Main characteristics of the ten sampling stations of the MERITE-HIPPOCAMPE cruise (13 April–14 May 2019) aboard the R/V *Antea* along a north-south transect in the Mediterranean Sea. The environmental conditions in these stations were detailed in Tedetti et al. (2023).

Station	Location	Latitude (N)	Longitude (E)	Bottom depth (m)	McLane sampling depth (m)	MultiNet sampling depth (m)
St1	Bay of Toulon (north)	43° 03.819'	5° 59.080'	91	20	20
St2	Toulon - Anthares (north)	42° 56.020'	5° 58.041'	1770	25	34
St3	Marseille - Julio (north)	43° 08.150'	5° 15.280'	95	55	58
St4	Bay of Marscille (north)	43° 14.500'	5° 17.500'	58	31	35
St9	North Balearic Front (offshore)	41° 53.508'	6° 19.998'	2575	20	20
St10	North Balearic Front (offshore)	40° 18.632'	7° 14.753'	2791	50	30
St11	North Balearic Front (offshore)	39° 07.998'	7° 41.010'	1378	40	30
St15	Gulf of Hammamet (south)	36° 12.883'	11° 07.641'	100	40	60
St17	Gulf of Gabès (south)	34° 30.113'	11° 43.573'	50	40	40